Cell Biology
Developmental Biology

Endosomal-lysosomal organellar assembly (ELYSA) structures coordinate lysosomal degradation systems through mammalian oocyte-to-embryo transition

Reviewed Preprint
v2 • January 31, 2025
Revised by authors

Reviewed Preprint
v1 • July 26, 2024

Yuhkoh Satouh, Takaki Tatebe, Isei Tanida, Junji Yamaguchi, Yasuo Uchiyama, Ken Sato

Laboratory of Molecular Traffic, Institute for Molecular and Cellular Regulation, Gunma University, Maebashi, Japan • Department of Cellular and Molecular Neuropathology, Juntendo University Graduate School of Medicine, Tokyo, Japan

eLife Assessment

This paper reports **important** findings on giant organelle complexes containing endosomes and lysosomes (termed endosomal-lysosomal organelles form assembly structures [ELYSAs]) present in mouse oocytes and 1- to 2-cell embryos. The data showing the localization and dynamics of ELYSAs during oocyte/embryo maturation are **convincing**. This work will be of interest to general cell biologists and developmental biologists.

https://doi.org/10.7554/eLife.99358.2.sa3

Abstract

Mouse oocytes undergo drastic changes in organellar composition and their activities during maturation from the germinal vesicle (GV) to meiosis II (MII) stage. After fertilization, the embryo degrades parts of the maternal components via lysosomal degradation systems, including autophagy and endocytosis, as zygotic gene expression begins during embryogenesis. Here, we demonstrate that endosomal-lysosomal organelles form large spherical assembly structures, termed ELYSAs, in mouse oocytes. ELYSAs are observed in GV oocytes, attaining sizes up to 7–8 μm in diameter in MII oocytes. ELYSAs comprise tubular-vesicular structures containing endosomes and lysosomes along with cytosolic components. Most ELYSAs are also positive for an autophagy regulator, LC3. These characteristics of ELYSA resemble those of ELVA (endolysosomal vesicular assemblies) identified independently. The signals of V1-subunit of vacuolar ATPase tends to be detected on the periphery of ELYSAs in MII oocytes. After fertilization, the localization of the V1-subunit on endosomes and lysosomes increase as ELYSAs gradually disassemble at the 2-cell stage, leading to further acidification of endosomal-lysosomal organelles. These findings suggest that the ELYSA/ELVA

maintain endosomal-lysosomal activity in a static state in oocytes for timely activation during early development.

Summary blurb

This study describes endosomal-lysosomal organellar assembly structures in mammalian oocytes, elucidating statistical alterations in their size, distribution, and correlation with lysosomal maturation.

Introduction

Fertilization triggers the dynamic remodeling of cellular components via zygotic gene expression as well as the degradation of cellular components from both maternal and paternal gametes[1]. After fertilization, maternal cytosolic proteins and RNAs are selectively degraded by the ubiquitin-proteasome system (UPS)[2] and specific RNA degradation systems[3, 4], respectively. Treatment with a proteasome inhibitor or knockdown of the zygote-specific proteasome assembly chaperone gene inhibits cytokinesis in zygotes, suggesting an essential role for the UPS in early development[5, 6]. Membrane components derived from each gamete are degraded by the lysosomal degradation system via autophagy and endocytosis[7, 8]. In mice, autophagic activity is relatively low in metaphase II (MII) oocytes, whereas it is rapidly upregulated approximately 4 h after fertilization, and LC3 (MAP1LC3: Microtubule-associated protein light chain 3)-positive structures appear throughout the cytoplasm. Autophagic activity decreases slightly before and after the 2-cell stage but remains high from the 4- to 8-cell stage[9]. Loss of Atg5 causes embryonic lethality at the 4- to 8-cell stages, suggesting that autophagy is essential for early mouse development. In contrast, some maternal plasma membrane (PM) proteins are internalized from the PM at the late 2-cell stage and are selectively degraded by lysosomes[10]. Endocytosis inhibitors prevent cell division in 2-cell embryos, suggesting that endocytosis plays a pivotal role in early development[10, 11]. Although lysosomal degradation systems are drastically upregulated after fertilization, their regulation remains unknown.

In *Caenorhabditis elegans*, the lysosomal activity in oocytes is upregulated by major sperm proteins secreted from sperms as the oocytes grow and mature[12]. In this process, translational arrest of mRNA coding the V1-subunits of vacuolar ATPase in oocytes is released by the stimulation of sperm-derived factors. Consequently, the V1-subunits are recruited to the Vo-subunits in the lysosomal membrane, enhancing lysosomal acidification. This process is known as lysosomal switching[12]. In mouse embryos, LysoTracker staining analysis suggests that lysosomal acidification is prominent at the 2-cell stage but not in MII oocytes and zygotes[13], raising the possibility that lysosomal switching takes place during mouse embryogenesis.

In this study, we aimed to investigate the dynamics of the endolysosomal system during mouse oocyte maturation and embryogenesis. We found that endosomes and lysosomes assembled to form spherical structures in germinal vesicle (GV)-stage oocytes, which became larger as they matured into MII oocytes. Ultrastructural analysis showed that these structures were large spherical membrane assemblies, including endosomes, lysosomes, and tubulo-vesicular structures located in the periphery of the PM. We refer to this structure as the Endosomal-LYSosomal organellar Assembly (ELYSA). The ELYSA contains several cytosolic constituents. While ELYSAs are disassembled in late-stage zygotes, immature endosomes and lysosomes gradually appear in the cytoplasm of early 2-cell stage embryos. Live imaging analysis showed that the signal of V1-subunit of V-ATPase on the acidic compartment became stronger during embryogenesis,

suggesting further acidification of lysosomes. These findings suggest that the ELYSA maintains low endosomal and lysosomal activities and acts as a waiting place for endolysosomal organelles to undergo fertilization-triggered activation toward embryogenesis.

Results

Endosomes and lysosomes coordinately form giant structures in MII oocytes

To examine the localization of endosomes and lysosomes in mouse MII oocytes, early or late endosomes were stained with anti-RAB5 or RAB7 antibody, respectively, and their localization was compared with that of lysosomes stained with anti-LAMP1 antibody. Giant structures harboring lysosomes with early and late endosomes were detected (**Fig. 1A**, **Supplementary Fig. 1**, Video 1). Although small punctate structures that are RAB5-positive but LAMP1-negative also spread over the cytosol, most giant structures were positive for RAB5 and LAMP1 (Video 1). Each giant structure in the MII oocytes was spherical, ellipsoidal, or concatenated with small spheres. These structures were located in the peripheral region just beneath the PM, excluding the metaphase plate region in proximity to the metaphase chromosomes. These structures were observed from the GV stage to the pronuclear-zygote (PN-zygote) stage but were mostly disassembled at the 2-cell stage. Dispersion and separation of RAB5 and LAMP1 signals after the first division indicated that these giant structures were transiently formed (**Fig. 1 B**). On the other hand, RAB5-positive and LAMP1-negative punctate structures tend to accumulate along with LAMP1-positive punctate structures larger than 1 μm at the late 2-cell stage.

Analyses of the number, size, and distribution of LAMP1-positive organelles were carried out by reconstituting three-dimensional objects using LAMP1-positive signals in immunocytochemically stained oocytes and embryos (**Supplementary Fig. 2**). Although the LAMP1 signals on the PM increased in the 2-cell stages, reconstitution of the objects was carried out only for the cytoplasmic fraction. The total number of the LAMP1-positive objects was highest at the GV stage, and it decreased toward the late 2-cell stage, with a significant difference compared to that in MII oocytes (**Fig. 2A**). Sorting of the objects based on their sizes (indicated with the diameters when converting the volume of each object to the corresponding sphere) revealed that the LAMP1-positive structures with diameters of 0.2–0.8 μm, which were prominent in GV oocytes, significantly decreased toward the MII stage, while the number of giant LAMP1-positive structures with diameters of 3–7 μm decreased during the post-fertilization changes at the early and late 2-cell stage relative to that in MII (**Fig. 2B**). The ratio of the number of the LAMP1-positive structures clearly indicated a drastic increase in giant structures with 5–7 μm diameter during GV to MII transition (**Fig. 2C**). The transiently increased LAMP1-positive structures with 9–10 μm diameter at the early 2-cell stage were observed as concatenated spheres that gathered upon cellular division; concurrently, prominent signals on the PM appeared, especially at the cleavage furrow and disappeared by the late 2-cell stage (**Fig. 2D, E**). The total volume of LAMP1-positive objects was highest in MII, and it decreased over the early and late 2-cell stages (**Fig. 2F**). LAMP1-positive structures with diameters of > 3 μm were also observed in GV oocytes, but those larger than 5 μm in diameter were rarely detected, and the total volume of LAMP1-positive structures larger than 3 μm in diameter in MII oocytes accounted for 51.3% of the total volume. The large population of the LAMP1-positive structures with diameters larger than 3 μm in MII transitioned to structures with diameters of 1–3 μm during the 2-cell stages, as indicated by the percentage of the volume of each object size relative to the total volume (**Fig. 2G**). The reconstitution of the objects above was conducted after the thresholding of the fluorescent intensity. On the other hand, objects with diameters of 6–7 μm in MII oocytes retained high intensity/volume, but those in GV oocytes or fertilized embryos revealed lower intensities (**Supplementary Fig. 3**).

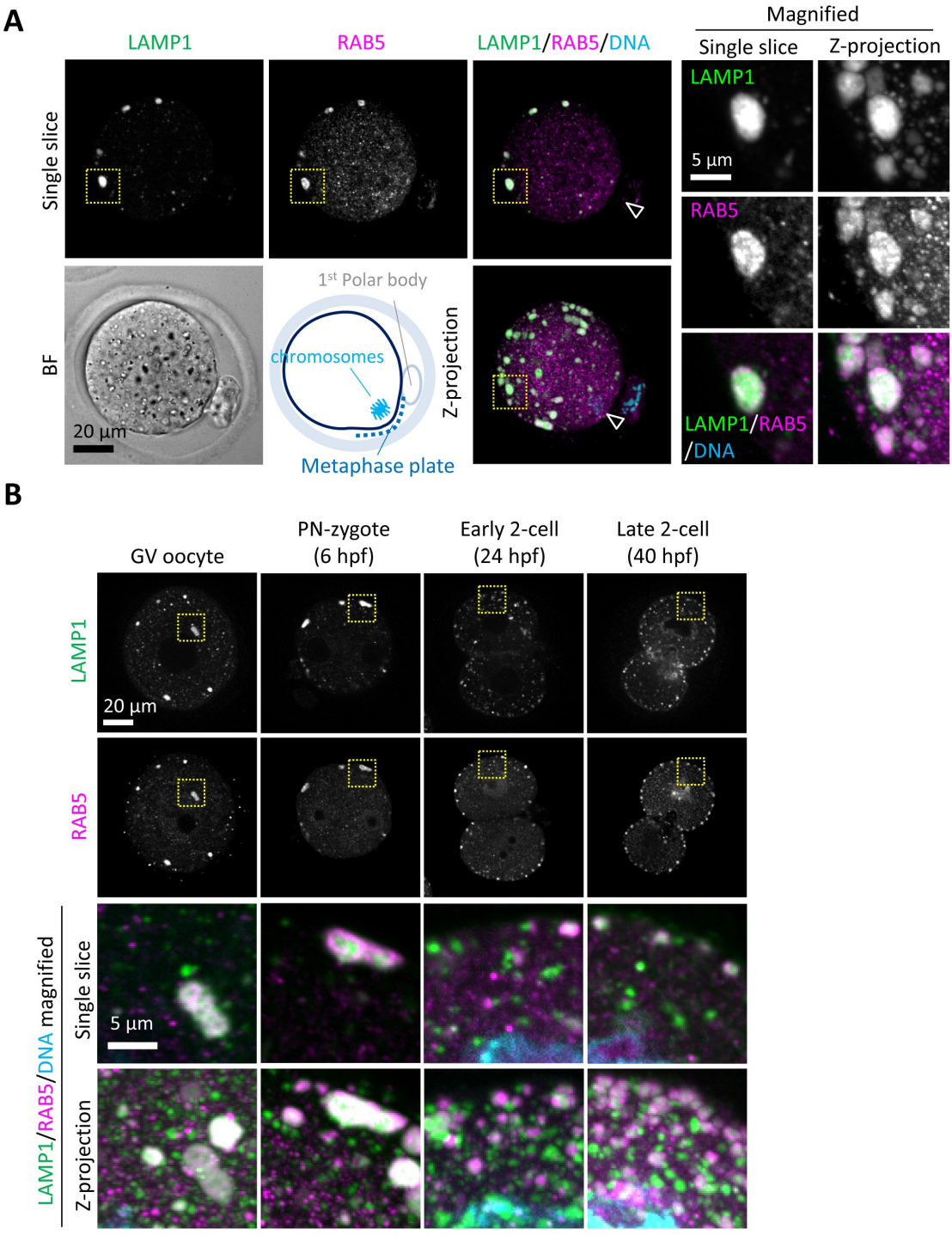

Fig. 1.

Endosomes and lysosomes form giant structures in the periphery of the oocyte plasma membrane

(A) Meiosis II (MII) oocytes were fixed and co-stained with anti-RAB5 and anti-LAMP1 antibodies. The schematic diagram indicates the location of oocyte chromosomes and metaphase plate in the MII oocytes. Arrowheads indicate the positions of oocyte chromosomes. Magnified regions (right) are indicated by yellow boxes. (B) Embryos at different stages were fixed and co-stained with anti-RAB5 and anti-LAMP1 antibodies. Hour(s) post-fertilization is indicated as hpf. DNA was stained with Hoechst 33342. Maximum intensity projection of confocal images at an axial scan range of 80 µm is shown as Z-projection images.

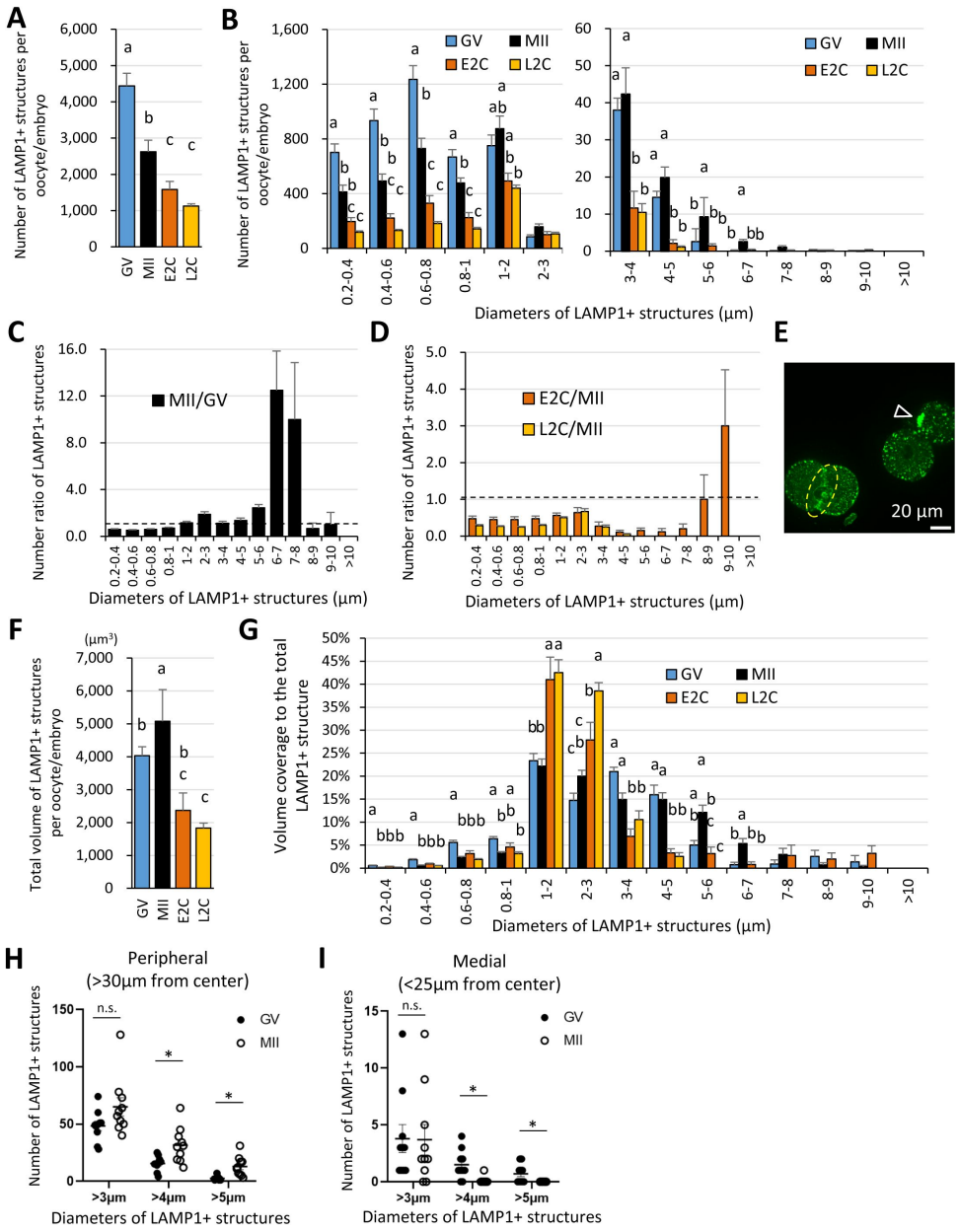

Fig. 2.

The giant structures are enlarged in the periphery of the MII oocyte PM during oocyte maturation

Germinal vesicle (GV) oocyte, MII oocyte, early 2-cell (E2C: 24 hpf), and late 2-cell (L2C: 40 hpf) embryos were fixed and stained with anti-LAMP1 antibody. Reconstituted three-dimensional objects for the LAMP1-positive organelles in 9 to 10 oocytes for each stage from more than three independent experiments were further analyzed for number, size, and distribution. (A) Averaged total number of LAMP1-positive objects per oocyte/embryo. (B) Numbers of the LAMP1-positive objects sorted by size (indicated by the diameters of spheres calculated from volumes). (C) Ratios of (B) for MII/GV to present changes during oocyte maturation. (D) Ratios of (B) for E2C/MII or L2C/MII to present post-fertilization changes. (E) A single confocal section image for E2C embryos, which have transient and concatenated objects upon cellular division (arrowhead) and a prominent signal on the PM of cleavage furrow (dotted circle). (F) Averaged total volume (μm^3) of the objects per oocyte/embryo. (F, G) Total volumes of the objects sorted by size, or the percentage of each fraction relative to the total LAMP1-positive object volume. (H, I) Numbers of large objects in GV or MII oocytes at a distance of > 30 μm (cellular peripheral) or < 25 μm (medial) from the cellular center. Groups with different letters are significantly different ($P < 0.05$, one-way ANOVA and Tukey's multiple comparison test). Error bars indicate SEM. Dot plots show mean ± SEM and asterisks indicate significant difference between two groups.

Furthermore, the analysis of object distribution for GV and MII oocytes indicated that MII oocytes had a greater number of LAMP1-positive structures with > 4 μm diameter in the cellular periphery, whereas GV oocytes had a greater number of these structures in the cellular medial regions (**Fig. 2H, I**). These results suggest that the giant LAMP1-positive structures are assembled and localized to the cellular periphery during oocyte maturation.

Endosomes, lysosomes, and tubulo-vesicular structures form an ELYSA

To clarify the internal structure of this giant structure containing lysosomes and endosomes in the MII oocytes, we observed these in MII oocytes with in-resin correlative light and electron microscopy (CLEM) using immunological reaction (immune in-resin CLEM) with anti-RAB7 and -LAMP1 antibodies[14, 15]. RAB7- and LAMP1-signals were well detected even in the ultrathin section (100 nm thickness) of the Epon-embedded MII oocyte, fixed with the mixture of 4% paraformaldehyde and 0.025% glutaraldehyde (GA), which showed similar distribution as that shown in **Fig. 1** and **Supplementary Fig. 4**. Toluidine blue staining in adjacent ultrathin sections revealed that the RAB7/LAMP1-double positive structures in the fluorescence observation were also positive for toluidine blue, with interspaces often found in the center of spheres (**Fig. 3A**). Confocal fluorescent images of the ultrathin sections clarified that RAB7-positive signals were frequently observed on the periphery of these LAMP1-positive signals. Electron microscopic analysis of the RAB7/LAMP1-double positive region in the ultrathin sections revealed that the RAB7/LAMP1-double positive structures are assemblies of tubulo-vesicular structures, with either vacuolated or filled interiors (**Fig. 3B**). The toluidine blue stain-positive structures were confirmed to match in size and peripheral distribution with those identified via RAB7/LAMP1 immunostaining, except for the metaphase plate, even under 2.5% GA conditions for precise ultrastructural observation (**Fig. 3C**, **Supplementary Fig. 5**, Video 2). Therefore, we examined the ultrastructural morphology of toluidine blue-positive giant structures in MII oocytes fixed with 2.5% GA. The results showed that tubular membrane vesicles with a short diameter of approximately 60.5 ± 15.9 nm assembled in the structure, with gaps in the cytoplasm of approximately 24.0 ± 6.7 nm. Some of the vesicles also harbored lysosome-like electron-dense contents, while others displayed multilamellar or multivesicular body-like structures, and mitochondria appeared to be absent (**Fig. 3D**). Based on these observations, we termed this membrane assembly the Endosomal-LYSosomal organellar Assembly (ELYSA).

An autophagy regulator, LC3, also accumulated in ELYSA

We next examined whether autophagy-related proteins are included in ELYSAs. LC3 is a key regulator of autophagy and often used as an autophagosome marker. It has been suggested that the autophagic activity is decreased in MII oocytes since puncta formation of transgenically-expressed a GFP fusion protein with LC3 disappeared at the MII stage[9]. Since GFP fluorescence may be quenched under acidic conditions, we examined the localization of LC3 in GV and MII oocytes by immunostaining with an anti-LC3 antibody. We found that LC3 hardly formed puncta in the cytoplasm, but part of the LC3 signal overlapped with ELYSA in both GV and MII oocytes (**Fig. 4A, B**), suggesting that LC3-positive membrane structures were also present in the ELYSA. Further analysis of such double-positive structures for the LC3 and LAMP1 antibodies indicated that their number decreased drastically, while their total volume did not change during oocyte maturation (**Supplementary Fig. 6A, B**). Analysis of double-positive structures indicated that their average diameter significantly shifted from 2.36 ± 0.31 μm (GV) to 3.78 ± 0.20 μm (MII). Moreover, LAMP1-positive structures smaller than 2 μm in diameter were rarely positive for LC3 (**Supplementary Fig. 6C, D**). On the other hand, analysis of the distance from the cellular geometric center indicated that they tended to be observed at the periphery of oocytes in both stages (more than 80% in > 30 μm in the MII oocyte), and no clear tendency of double positivity was observed along the distance (**Supplementary Fig. 6E, F**). A similar trend was observed for

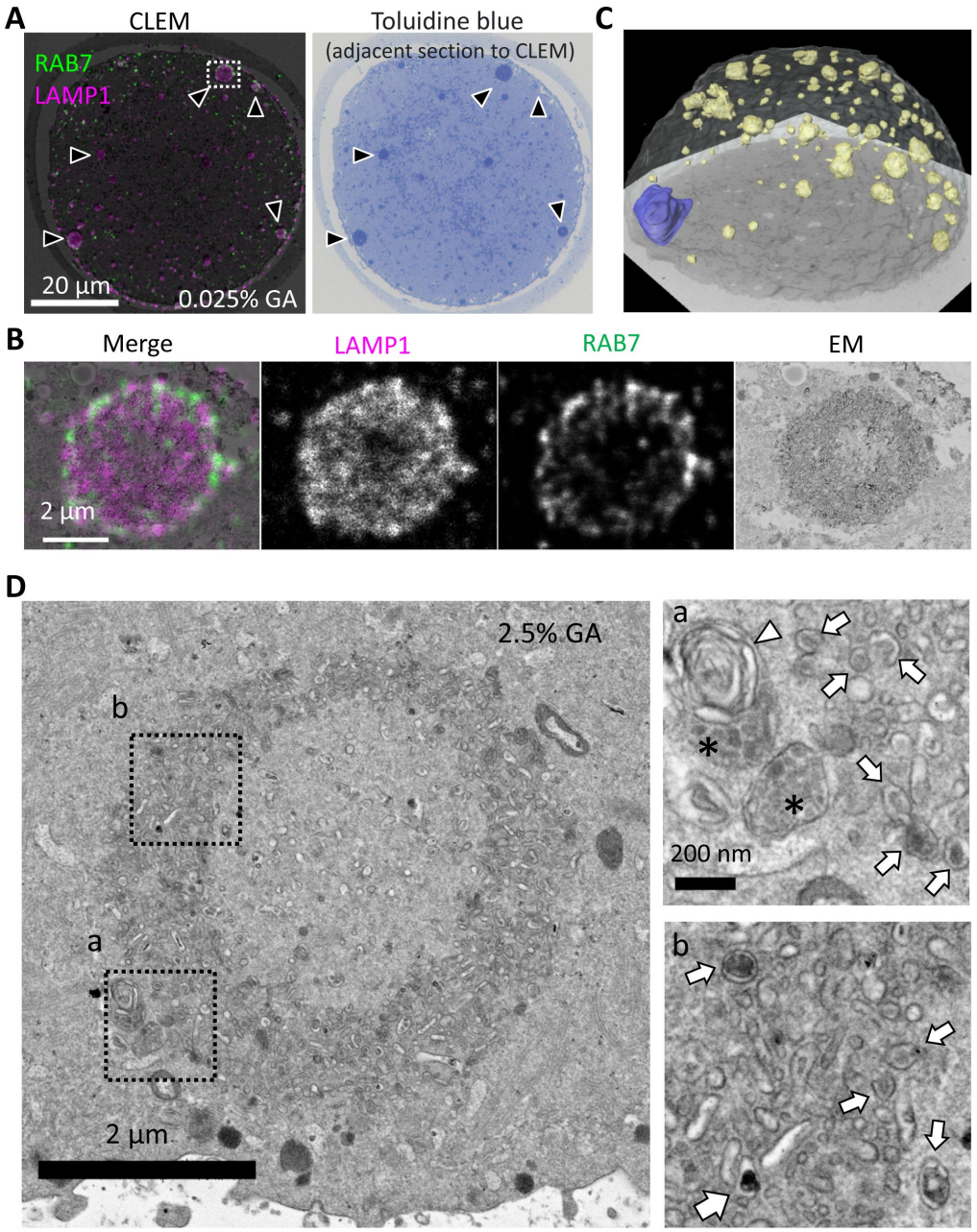

Fig. 3.

Endosomal-lysosomal organelles form assembly structures, ELYSA

(A) The internal structure of the giant structure in MII oocytes was analyzed by correlative light and electron microscopy (CLEM) analysis using anti-RAB7 and anti-LAMP1 antibodies. A merged image of immunostaining and electron microscopy (EM) is indicated (left), and a toluidine blue staining image of the adjacent thin section (right) is indicated. Black arrowheads indicate the giant structures positive for RAB7/LAMP1/toluidine blue staining. Note that RAB7/LAMP1 staining is indicated in a pseudo-color. (B) The fluorescent distribution of RAB7/LAMP1 immunostaining was analyzed with deconvolution confocal microscopy. Note that RAB7/LAMP1 staining is indicated in pseudo-color. (C) A series of images of toluidine blue-stained serial semi-thin sections of the Epon-embedded MII oocyte were reconstructed in 3D. Based on the images obtained, chromosomes were segmented blue, toluidine blue-positive structures were segmented yellow, and the oocyte PM was segmented white. (D) The internal structures of the toluidine blue-positive structure, ELYSA, were observed using conventional EM of oocytes fixed with 2.5% glutaraldehyde (GA). Magnified regions in a or b (right) are indicated by boxes (left). Arrows, arrowheads, or asterisks indicate vesicles harboring high electron density contents and multilamellar or multivesicular structures, respectively. ELYSA, endosomal-lysosomal organellar assembly.

RAB5 and LAMP1 double-positive structures, while the RAB5 signals tended to overlap with LAMP1 signals more specifically at the cellular periphery than LC3, even in the GV stage (**Supplementary Fig. 6G, H**).

ELYSA enlargement proceeds in an actin dependent manner

The localization of LAMP1-positive structures at the perinuclear (medial) region before oocyte maturation and the specific localization at the cell periphery after maturation (**Fig. 2H, I**) is similar to the redistribution of the endoplasmic reticulum (ER) and the formation of cortical ER clusters. Fitzharris et al. showed that the inhibition of actin cytoskeleton polymerization disturbs ER migration and cortical ER cluster formation[16]. Thus, we examined the involvement of cytoskeletons in ELYSA formation by adding latrunculin A (LatA) or cytochalasin B (CCB) as inhibitors of actin polymerization and nocodazole (Noco) as an inhibitor of microtubule formation during *in vitro* maturation (IVM). While all the drugs inhibited polar body extrusion and metaphase plate formation as reported previously[16], co-immunostaining of LC3- or RAB5-antibody with LAMP1-antibody revealed their persistent colocalization in ELYSAs (**Fig. 5A**, **Supplementary Fig. 7**).

Three-dimensional object analysis of the oocytes with or without cytoskeletal inhibitor treatment indicated that the total number of LAMP1-positive structures was increased only by CCB, and the total volume of the structures was unaffected (**Supplementary Fig. 8**). We then classified LAMP1-positive structures by their diameters and found that the number of structures with diameters of 0.8–2.0 μm increased when oocytes were treated with LatA and CCB; very few structures with diameters of 4–7 μm that corresponded to the enlarged ELYSAs were detected upon treatment with actin polymerization inhibitors, not the tubulin inhibitor (**Fig. 5B**). Further examination of the distance from the cell center of each LAMP1-positive structure with a diameter larger than 4 μm in IVM oocytes indicated that only the actin polymerization inhibitors reduced the number of large structures at the cell periphery but not in the cellular medial region (**Fig. 5C, D**).

V1 component of V-ATPase partially localizes to the periphery of ELYSAs in oocytes

We studied the relationship between ELYSA formation and endosomal/lysosomal acidification in oocytes. V1A is a component of the V1 subunit of V-ATPase, which is associated with the outer lysosomal membrane and drives endosomal/lysosomal acidification. We used LAMP1-EGFP mRNA to observe ELYSA behaviors during oocyte maturation, with ATP6V1A-mCherry mRNA (V1A-mCherry: a core component of V-ATPase fused with the mCherry marker) to further examine the V1 subunit localization on ELYSAs. The mRNAs were injected into GV oocytes, and the oocytes were applied to IVM.

Three-dimensional object analysis for the matured (MII) oocytes expressing LAMP1-EGFP revealed a larger number of smaller LAMP1-positive structures (diameter of 0.2–0.4 μm) and a smaller number of structures with diameters of 0.6–1.0 μm, compared to immunostaining (**Fig. 2**), but not significant difference in larger size (**Supplementary Fig. 9**). Live-cell imaging of LAMP1-EGFP fluorescence captured the dynamics of LAMP1-positive organelles during oocyte maturation, notably demonstrating its stable expression after germinal vesicle breakdown (GVBD, 2–3 h after initiation of IVM), and revealed that the enlargement of ELYSAs larger than 5 μm in diameter occurred through the sequential assembly of smaller ELYSAs that constantly migrated and contacted each other (**Fig. 6A**, Video 3).

We then analyzed the localization of V1A-mCherry in the oocytes after IVM. Although it was indistinguishable whether V1 subunit molecules or V1 subunit-positive compartment were recruited to ELYSAs, V1A-mCherry signals were largely distributed on the ELYSA surface and

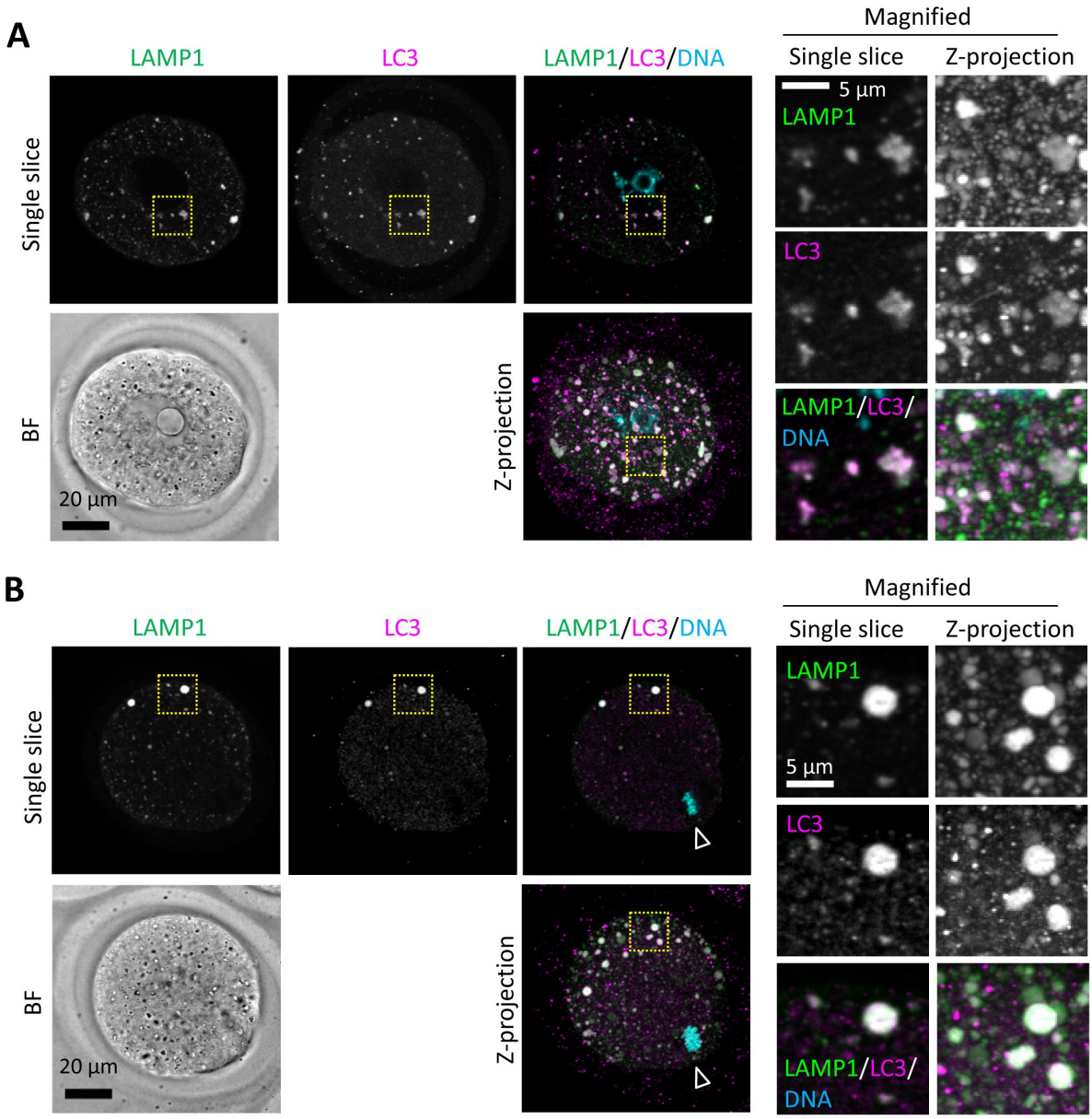

Fig. 4.

An autophagy regulator LC3 is detected in ELYSA

Germinal vesicle (GV) (A) and MII (B) oocytes were fixed and co-stained with anti-LC3 and anti-LAMP1 antibodies. Magnified regions (right) are indicated by yellow boxes. DNA was stained with Hoechst 33342. Arrowheads indicate the positions of oocyte chromosomes. Maximum intensity projection of confocal images at an axial scan range of 80 µm is shown as Z-projection images.

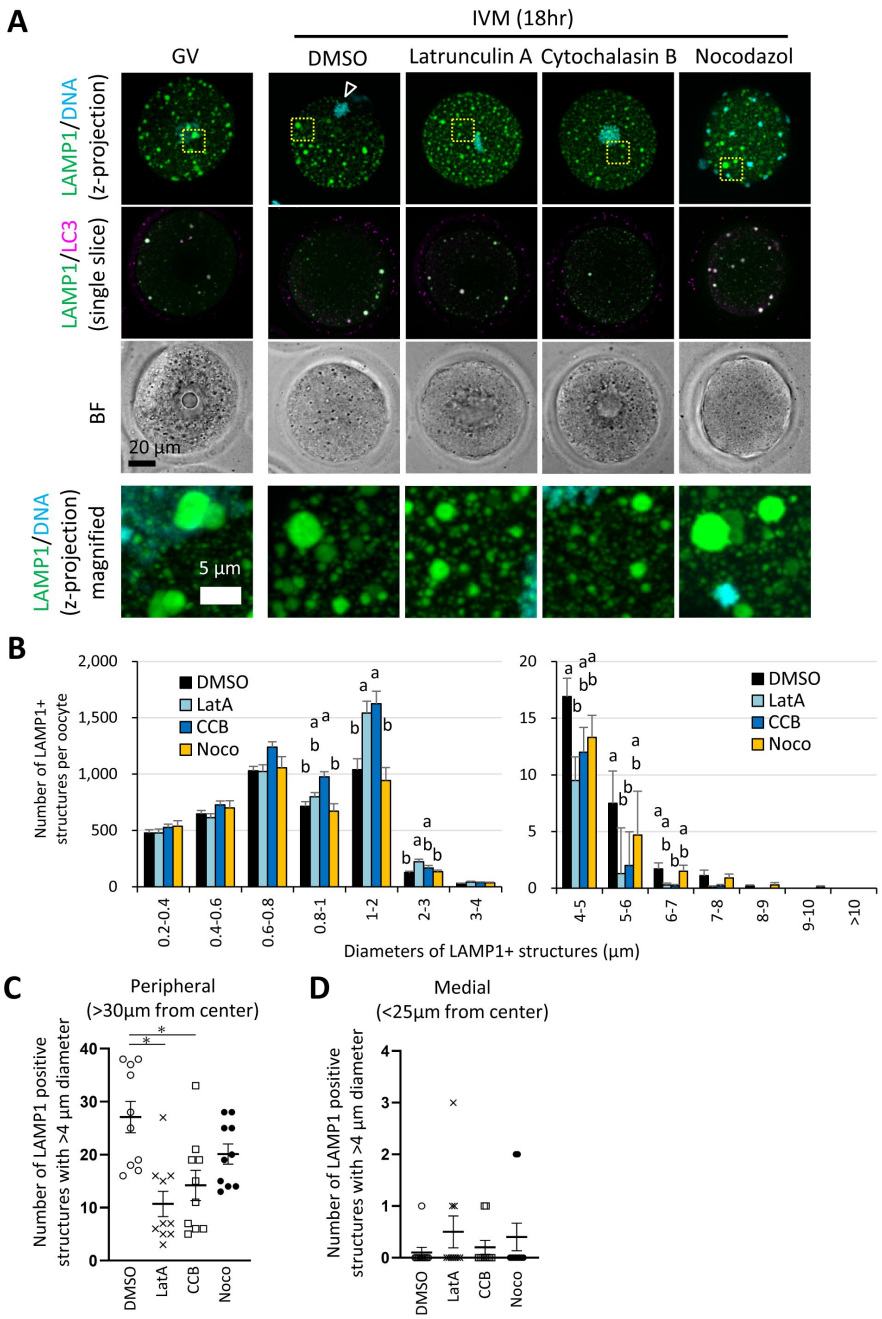

Fig. 5.

Enlargement of ELYSA and its redistribution to the cell periphery occur in an actin cytoskeleton-dependent manner

GV oocytes were incubated for *in vitro* maturation (IVM) for 18 h with or without actin polymerization inhibitors (10 μM latrunculin A or cytochalasin B) or a tubulin inhibitor (20 μM nocodazole), then fixed and co-stained with anti-LC3 and anti-LAMP1 antibodies. The reconstituted objects for LAMP1-positive organelles in 10 oocytes for each treatment from more than three independent experiments were analyzed for the number, size, and distribution. (A) Maximum intensity projection of confocal images at an axial scan range of 80 μm is shown as Z-projection images. DNA was stained with Hoechst 33342. Arrowheads indicate the metaphase plate. (B) Average total LAMP1-positive object number per oocyte after sorting the objects by size (indicated by the diameters of spheres calculated from volumes). (C, D) Numbers of objects with diameters > 4 μm in oocytes at a distance of > 30 μm or < 25 μm from the cellular center. Groups with different letters are significantly different ($P < 0.05$, one-way ANOVA and Tukey's multiple comparison test). Error bars indicate SEM. Dot plots are indicated with mean ± SEM.

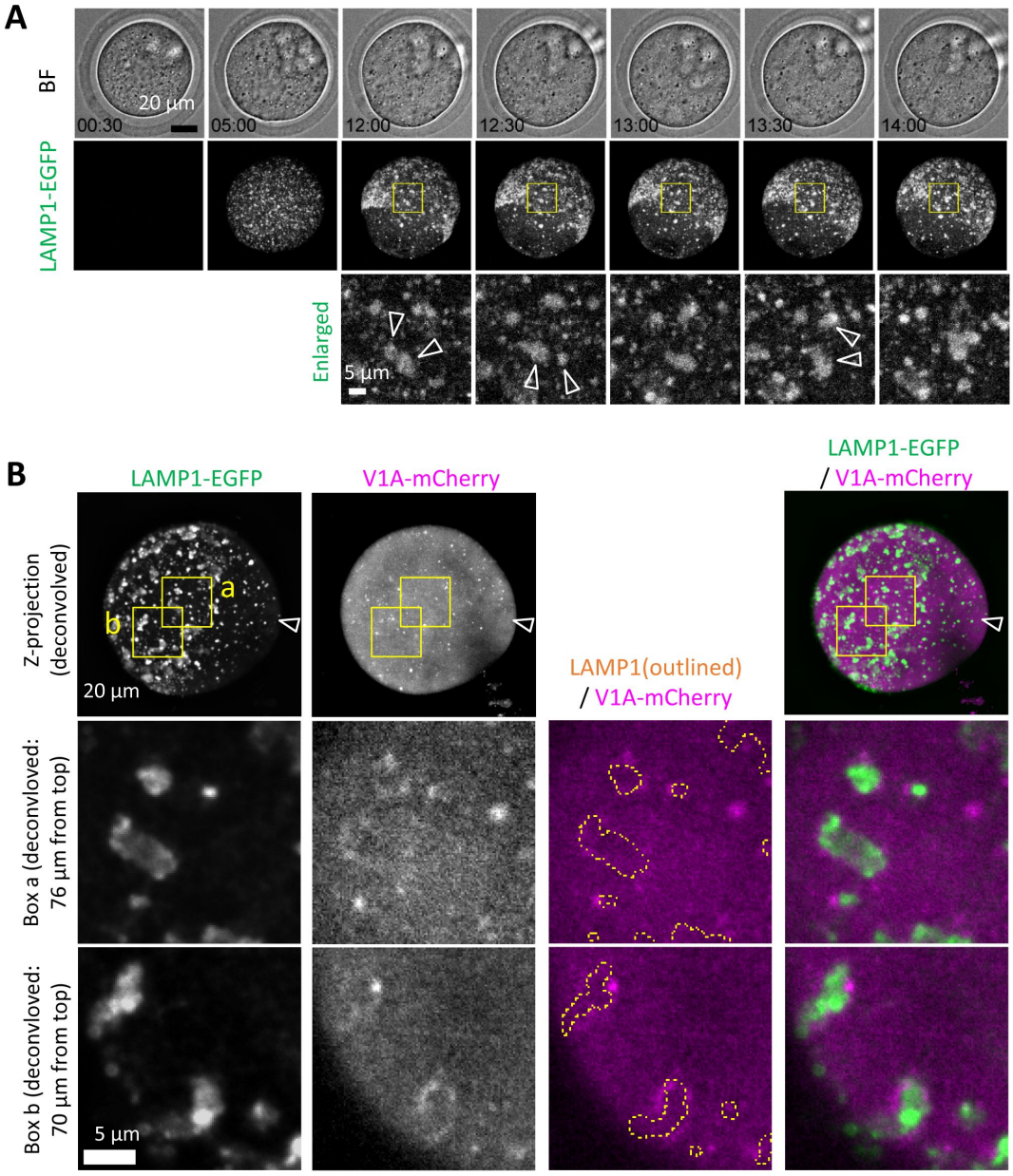

Fig. 6.

Assembly of ELYSA during migration and limited interaction with the acidification machinery

(A) Snapshots of a time-lapse observation for EGFP fluorescence of GV oocytes injected with *Lamp1-EGFP* and *V1A-mCherry* mRNA are indicated. Maximum intensity projection of confocal images with a height of 40 μm (bottom half of the oocyte) are shown. Magnified perinuclear regions (right) are indicated by yellow boxes. Arrowheads indicate assemblies that adhere to each other in the subsequent frame. (B) Maximum intensity projection of deconvolved confocal images at an axial scan range of 80 μm is shown as Z-projection images. Magnified regions are indicated by yellow boxes (a, b) and the LAMP1-EGFP organelle regions are indicated by yellow dotted line.

rarely observed within ELYSAs in deconvolved confocal images (**Fig. 6B**, Video 4).

Acidification of lysosomes is facilitated as ELYSA disassembly proceeds in embryos

We examined the relationship between ELYSA disappearance and the emergence of acidic membrane compartments during early development. LysoSensor probes exhibit increased fluorescence in a pH-dependent manner upon acidification and enable the semi-quantitative analysis of cellular acidic compartments, whereas LysoTracker probes exhibit non-pH-dependent fluorescence. We first co-stained oocytes and embryos at various stages with LysoTracker Red and LysoSensor Green (in the same medium drop). LysoTracker showed a pronounced puncta-like signal after the 2-cell stage, as previously reported[13]. In contrast, the ELYSAs in GV and MII oocytes were clearly identified by LysoSensor, whereas LysoTracker only produced a very dim signal. Thus, the ratio of LysoTracker/LysoSensor fluorescent intensities in the cytoplasm of each stage embryo indicated that ELYSAs were present at a low ratio. In contrast, embryos at the 4-cell stage and beyond displayed small punctate signals with a higher ratio (**Fig. 7**). A comparison between LysoTracker and V1A-mCherry signals showed that these fluorescent signals colocalized well on small bright vesicles but not on the ELYSA. Both LysoTracker and V1A-mCherry puncta were reduced in embryos cultured in the presence of bafilomycin A_1, which inhibits the H^+ translocation of V-ATPase (**Supplementary Fig. 10**). This suggests that LysoTracker detects membrane compartment acidification. However, it may not sufficiently capture this process within the ELYSA. In contrast, the results using LysoSensor suggest that lysosomes within the ELYSA were not completely neutralized and remained acidic at a lower level, even though V1A was difficult to localize.

When LAMP1-EGFP mRNA was injected into fertilized oocytes, it was difficult to visualize the lysosomes due to the presence of a population that migrates onto the PM during the 2-cell stage. Thus, to examine the spatiotemporal relationship between V1A localization and lysosomal acidification during embryogenesis, we injected V1A-mCherry mRNA into PN zygotes and cultured them in the presence of LysoSensor. It should be noted that stable detection of LysoSensor and V1A-mCherry fluorescence required 4–8 h. In this process, localization of V1A signal to lysosomes was rarely observed until ELYSA disappearance or disassembly throughout the PN-zygote stage, but rapidly enhanced in the early 2-cell embryo stage. LysoSensor-positive punctate structures, where V1A-mCherry signal colocalize, increased in number during the transition from early to late 2-cell stage, indicating that lysosomal acidification is promoted after ELYSA disappearance (**Fig. 8**, Video 5).

Low-level cathepsin-dependent proteolytic activity was maintained in ELYSA

Cathepsins are mainly responsible for the proteolytic activity in lysosomes. We visualized the proteolytic activity of cathepsin B, the expression of which has been confirmed in mouse embryos[13]. Mouse oocytes and embryos at various stages were simultaneously collected and stained with Magic Red Cathepsin B staining solution to examine their relationship with the ELYSA. Magic Red staining showed that proteolytic activity was detected not only in the small, isolated membrane structures (mature lysosomes) but also in the ELYSA in the GV and MII oocytes, whereas small punctate structures were predominantly stained in other stages (**Fig. 9A**, **Supplementary Fig. 11A**). The intensity plots of LysoSensor and Magic Red fluorescence revealed that the proteolytic activity indicated by the Magic Red signal in the ELYSA was detected, but not as strong as that in isolated punctate structures (lysosomes) in the GV and MII oocytes, and in developing embryos (**Fig. 9B**, **Supplementary Fig. 11B, C**).

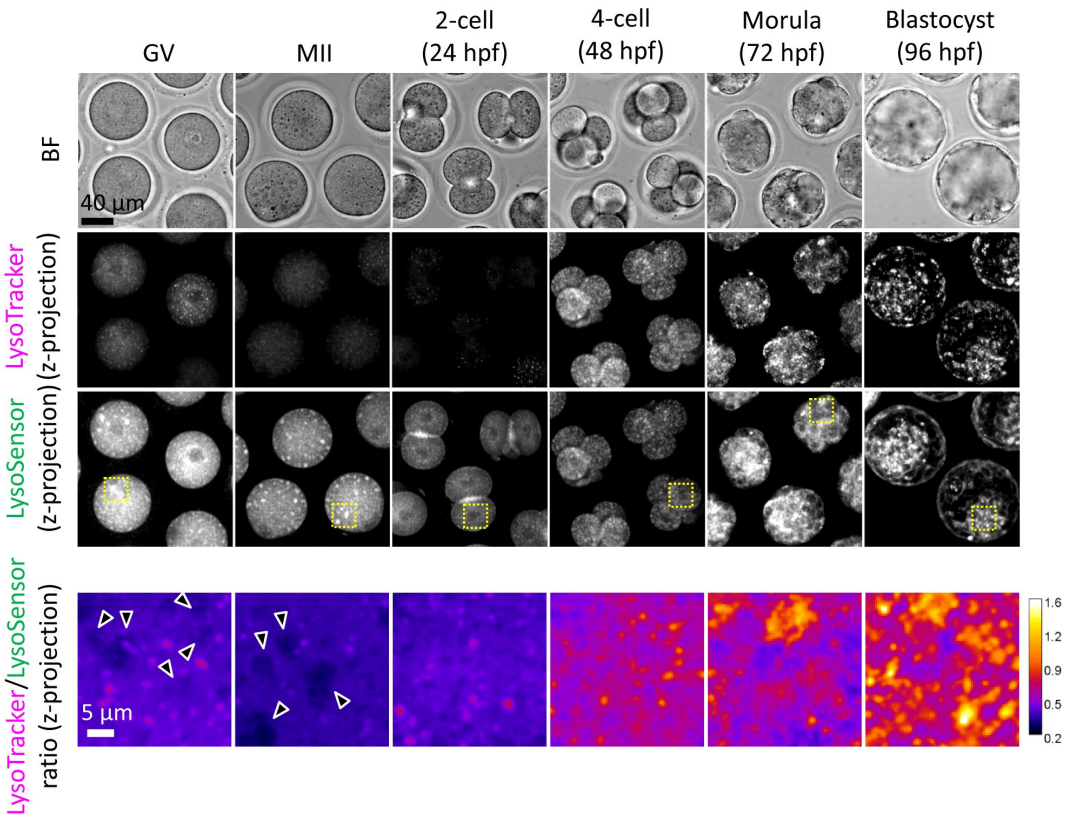

Fig. 7.

Endosomes and lysosomes in the ELYSA are weakly acidified, but further acidification occurs after the 4-cell stage

Oocytes and embryos at different stages were stained in the same drop for LysoSensor Green and LysoTracker Red staining analysis, and confocal images were acquired. Averaged intensity projection of confocal images at an axial scan range of 80 µm is shown as Z-projection images. Magnified ratiometric image for LysoTracker/LysoSensor fluorescence of cytosolic regions indicated by yellow boxes are presented as “fire” look up table images at the bottom. Arrowheads indicate ELYSAs recognized with LysoSensor.

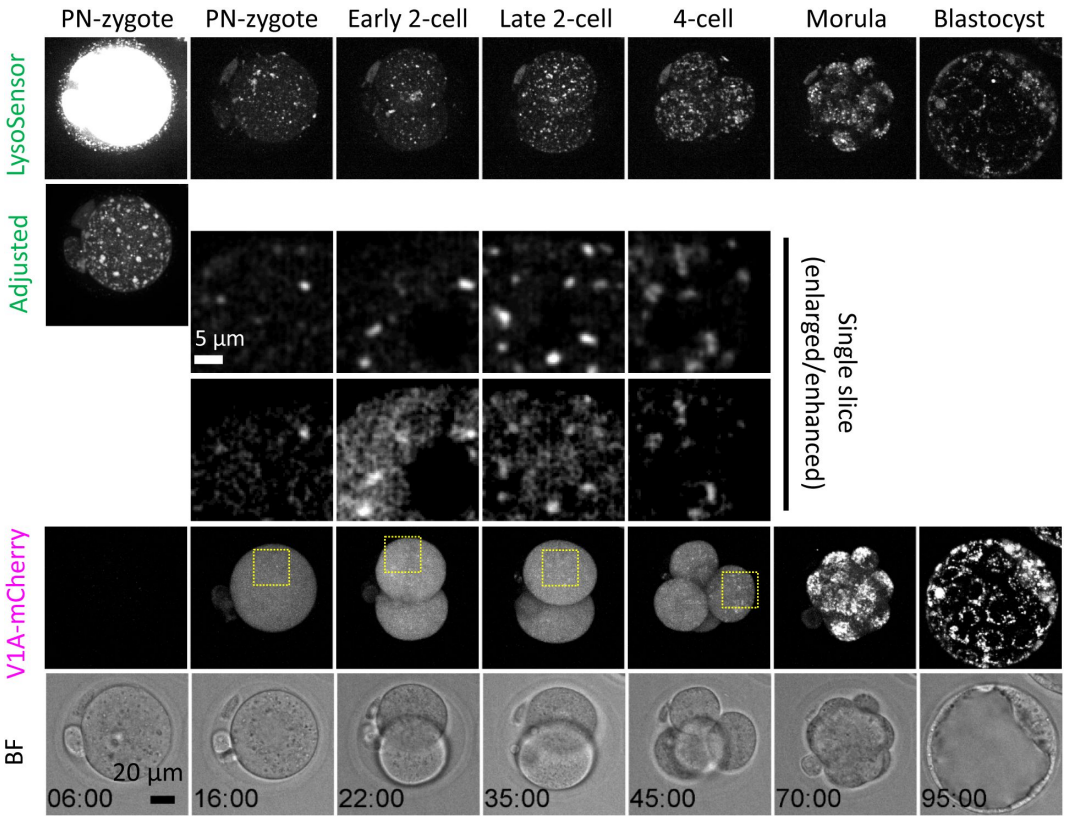

Fig. 8.

ATP6V1A localization on acidic compartments increases as ELYSAs are disassembled

Embryos injected with *V1A-mCherry* mRNA (at 3 hpf) were incubated to the blastocyst stage in the presence of LysoSensor Green. Snapshots of a time-lapse observation of a representative embryo are shown as maximum intensity projection of confocal images with a height of 80 µm unless otherwise specified. Magnified perinuclear regions are indicated by yellow boxes.

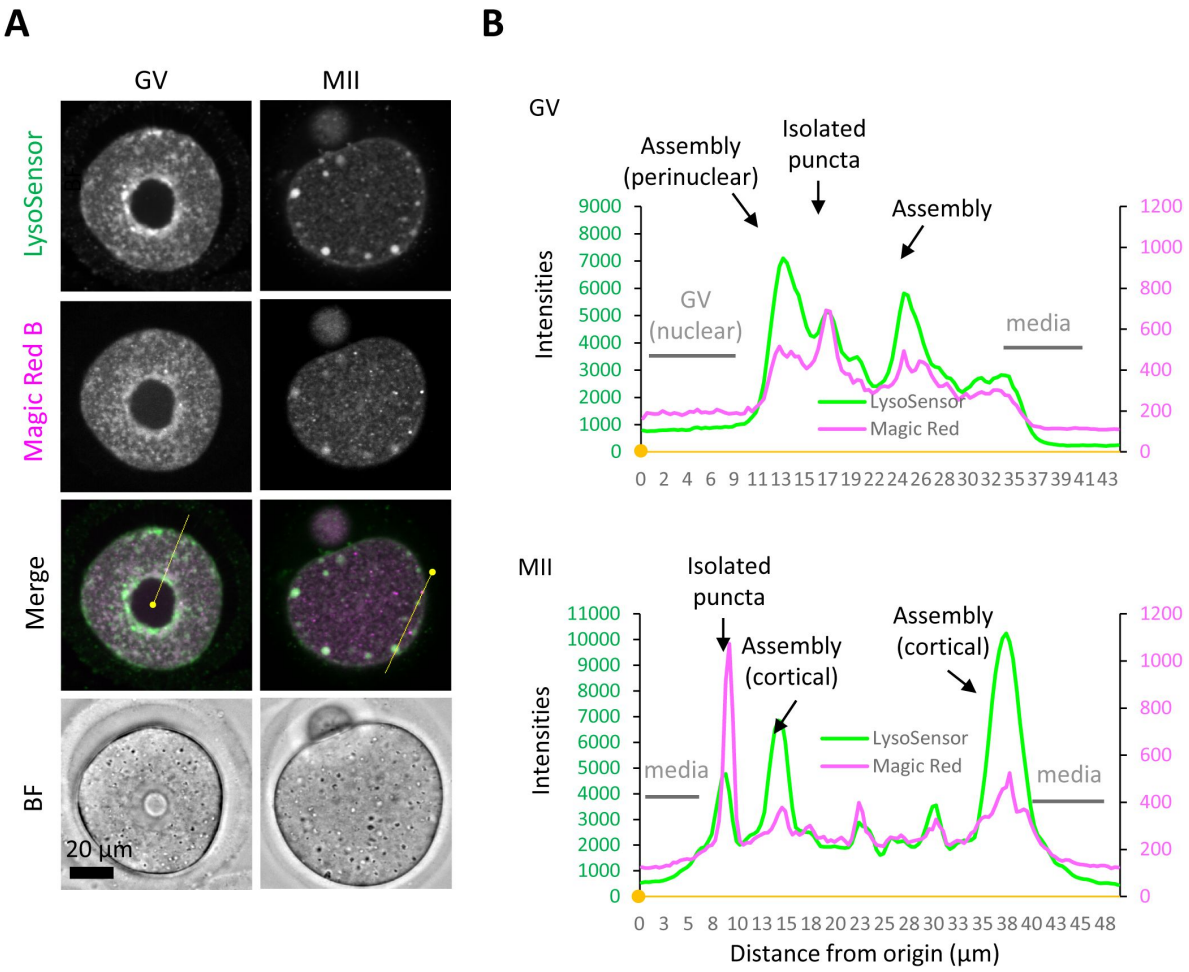

Fig. 9.

Proteolytic activity of cathepsin B is maintained at a relatively low level in the ELYSA

(A) GV and MII oocytes were stained in the same drop for LysoSensor Green and Magic Red Cathepsin B staining analysis, and confocal images were acquired. (B) Fluorescent intensities of LysoSensor and Magic Red on the yellow lines indicated in (A) are indicated by a line plot. Small, filled dots indicate the origin (0 µm) in distance.

Discussion

In this study, we identified a large spherical structure, the ELYSA, consisting of endosomes, lysosomes, LC3-positive structures, and various vesicular-tubular structures in mouse oocytes. Small ELYSAs are present in GV oocytes and increase in size (3 to 7 μm in diameter) through assembly at the cell periphery in an actin-dependent manner during oocyte maturation and occupying more than half the volume of the LAMP1-positive fraction in MII oocytes. After fertilization, as ELYSAs gradually disassemble in zygotes, punctate structures positive for either RAB5- or LAMP1-signal alone appear in the cytoplasm of embryos at the early 2-cell stage. The number of membrane structures positive for V1A-mCherry increase upon ELYSA disassembly, indicating further acidification of the endosomal/lysosomal compartment. These results suggest that the ELYSA functions as a reservoir that accumulates endosomal and lysosomal compartments at the periphery of the cell cortex and maintains their activities in a static state until embryogenesis following fertilization.

We studied the dynamics and activity of endosomes and lysosomes in mouse oocytes and embryos and found that some oocyte PM proteins are internalized from the PM at the late 2-cell stage and are selectively degraded in lysosomes[10]. In this process, we noted that lysosomes were not well stained by LysoTracker until the early 2-cell stage, but their signals became stronger from the late 2-cell stage, suggesting the existence of a mechanism underlying developmentally regulated endosomal/lysosomal activation during embryogenesis[10, 13]. Notably, ELYSAs were stained with toluidine blue and LysoSensor, suggesting that these structures were acidified to some extent (**Fig. 3**, 7). In addition, Magic Red, which reflects cathepsin B activity, weakly stained ELYSAs (**Fig. 9**). These observations indicate that lysosomes in ELYSAs have some activity, albeit at low levels. Mouse oocytes accumulate several maternal constituents, including proteins, lipids, and mRNA, and grow to approximately 75 μm in diameter. In addition, oocytes must remain at the GV and MII stages for an extended period to maintain their quality until fertilization. In such situations, lysosomal degradation activity may be suppressed to a relatively low level by the ELYSA, while nutrient uptake, storage, and protein synthesis are predominantly upregulated in growing oocytes. Furthermore, we found that the V1-subunit signals were largely detected on the periphery of ELYSAs but not in their interior in oocytes (**Fig. 6**). Thus, it is possible that ELYSA formation prevents the localization of V1-subunits on the lysosomal membrane inside the ELYSA.

Ultrastructural analysis revealed that the ELYSA consists of outer and inner membrane assembly layers containing several endosomes and lysosomes, respectively (**Fig. 1**, **3**). Considering the large number of RAB5-positive and LAMP1-negative punctate structures in MII oocytes, these layers may also reflect the assembly mechanism of the ELYSA. On the contrary, upon disassembly of the ELYSA, endosomes and lysosomes are expected to be released from the ELYSA earlier and later, respectively. This may explain the time lag between fertilization and lysosomal acidification beginning at the early 2-cell stage. Since the ELYSA appears to contain cytosolic constituents, it may accommodate some cytosolic constituents as a capsule to provide nutrition or signaling factors for development.

ELYSAs were distributed relatively widely in the GV oocyte, then specifically located at the periphery of the oocyte cell cortex, except in the MII cell plate in the MII stage (**Fig. 1**, **2** **Supplementary Fig. 6**). This change in distribution is reminiscent of that of the ER and cortical ER clusters, whose distribution is regulated by the actomyosin system[16]. In fact, the treatment with actin cytoskeleton polymerization inhibitors, but not a tubulin polymerization inhibitor, prevented the redistribution of ELYSAs from the cellular medial region to the cell periphery in oocytes (**Fig. 5**). The former treatment increased the number of small LAMP1-positive organelles but reduced the size of ELYSAs in oocytes (**Fig. 5**). These results suggest that actin cytoskeleton is involved in the assembly of smaller (< 2 μm in diameter) LAMP1-positive

organelles for the enlargement of ELYSAs in the cell periphery. Our detailed imaging analysis showed that lysosomal acidification is promoted simultaneously with the detection of the V1-subunits on lysosomes during ELYSA disassembly in late zygotes and is further facilitated from the 2- to 4-cell stage and is enhanced after the morula stage (**Fig. 8**, **Supplementary Fig. 10**). These findings suggest that lysosomal acidification and maturation are linked to the ELYSA disassembly. Notably, minor and major zygotic gene activation in mouse embryos occur at the 1- and 2-cell stages, respectively, implying that lysosomal degradation of maternal components is coupled with zygotic gene expression to promote embryogenesis[17]. Fertilization appears to trigger ELYSA disassembly, but the downstream signaling pathways remain to be identified and warrant further research.

Very recently, after sharing this ELYSA paper as a preprint in 2023[18], Zaffagnini et al. reported the endolysosomal vesicular assemblies (ELVAs), which resemble ELYSAs, in mouse oocytes[19]. The ELVA is defined as super-organelles containing endosomes, lysosomes, autophagosomes, and proteasomes along with cytosolic proteins, which sequesters detrimental protein aggregates inside and degrade them upon oocyte maturation[19]. Consistencies between the ELYSA and the ELVA in their contents and actin-dependent dynamics during oocyte maturation/embryogenesis strongly suggest that ELYSAs and ELVAs are identical structures[19], assuring the solidity of these findings in this paper. Zaffagnini et al. also observed the accumulation of proteasomes and ubiquitinated proteins in ELVAs and demonstrated that the depletion of a RUN and FYVE domain-containing protein 1 (RUFY1) protein from oocytes by the Trim-Away method causes disappearance of ELVAs, suggesting that RUFY1 is involved in the ELVA assembly. Analysis of *Rufy1*-knockout ELVA/ELYSA free oocytes is awaited to elucidate the physiological role of ELVAs or probably ELYSAs. They also suggested that ELVAs sequester and degrade specific proteins that is known to be aggregate and cause diseases, including proto-oncogene receptor tyrosine kinase KIT, upon oocyte maturation[19]. Complementary to their findings, our study revealed that the recruitment of the V1-subunit is limited on ELYSAs in oocytes but enhanced on the isolated LAMP1-positive vesicles after late 2-cell stage. These findings support a hypothesis that ELYSA has a multimodal function, keeping endosomal and lysosomal compartments at a relatively static state and supplying these membrane compartments as a reservoir for embryogenesis.

Inhibition of lysosomal acidification by bafilomycin A_1 treatment arrests embryogenesis at the 4–8-cell stage, while inhibition of cathepsin activity using a mixture of E64d and pepstatin A blocks embryogenesis at the 8-cell or morula stage[13]. In contrast, the inhibition of endocytosis by Pitstop2 treatment causes arrest at the 2-cell stage[10]. These differences may imply that at the 2-cell stage, the endocytic activity is more important than the lysosomal degradation activity, which is essential at later stages. However, insights from this study shed light on the correlation between increased endocytic/autophagic activity and lysosomal maturation through ELYSA disassembly and the potential significance of minor lysosomal maturation in the early phase of embryogenesis.

The relationship between such endocytic/autophagic activities in early-stage embryos and the embryonic developmental potential has been recently studied. Using GFP-LC3 as an indicator of autophagic activity, Tsukamoto et al. found that aged oocytes from 14- to 15-month-old mice had lower autophagic activity than those from younger mice, probably due to decreased lysosomal activity. Females transplanted with embryos with high autophagic activity at the 4-cell stage have a significantly higher litter size ratio than that of control females[20]. Analysis of ELYSA formation and disassembly in aged oocytes and embryos may be a useful tool for determining oocyte quality by examining appropriate regulation of endosomal/lysosomal activities.

Methods

Animal experiments and strains

Neither randomization nor blinding was used for animal selection (8–16-week-old). All experimental protocols involving animals were approved and performed in accordance with the guidelines of the Animal Care and Experimentation Committee of Gunma University (Approval No. 22-076). Hybrid B6D2F1 mice were purchased from the Japan SLC (Hamamatsu, Japan)

Antibodies and inhibitors

The following primary antibodies were used: rabbit monoclonal anti-RAB5 (C8B1; 3547; Cell Signaling Technology, Danvers, MA, USA), rabbit monoclonal anti-RAB7 (D95F2; 9367; Cell Signaling Technology), rat monoclonal anti-mouse LAMP1 (1D4B; sc-19992; Santa Cruz Biotechnology, Dallas, TX, USA), and mouse monoclonal anti-rat LC3 (Clones 4E12; M152-3; Medical and Biological Laboratories, Tokyo, Japan). The following secondary antibodies were used: goat anti-rabbit IgG (H+L) conjugated with Alexa Fluor 555 (A-21428; Thermo Fisher Scientific, Waltham, MA, USA), goat anti-rat IgG (H+L) cross-adsorbed secondary antibody conjugated with Alexa Fluor 488 and 647 (A-11006 and A-21247, respectively; Thermo Fisher Scientific), and goat anti-mouse IgG (H+L) cross-adsorbed secondary antibody conjugated with Alexa Fluor 546 (A-11030; Thermo Fisher Scientific). The following inhibitors or solutions were used for IVM or embryonic culture assays: dimethyl sulfoxide (DMSO) (13406-55; Nacalai Tesque, Kyoto, Japan); latrunculin A actin polymerization inhibitor that binds to monomer actin (428021; Sigma-Aldrich, St. Louis, MO, USA); cytochalasin B, an actin polymerization inhibitor that binds to the plus-end of polymerized actin (C6762; Sigma-Aldrich); and nocodazole, a tubulin polymerization inhibitor that binds to β-tubulin (M1404; Sigma-Aldrich). Stock solutions of latrunculin A, cytochalasin B, or nocodazole were prepared by solubilizing each in DMSO at 200× concentration for the assays. Bafilomycin A_1 was dissolved in DMSO (L266; Dojindo, Kumamoto, Japan) at a final concentration of 25 nM.

Oocyte preparation

GV oocytes were collected from the ovaries of female mice 46 h after injection with pregnant mare serum gonadotropin or an anti-inhibin antibody (CARD HyperOva; Kyudo, Kumamoto, Japan)[21]. Antral follicles were suspended in 30 µL of FHM medium drops (Sigma-Aldrich) covered with liquid paraffin (Nacalai Tesque), punctured using 26G needles (Terumo, Tokyo, Japan), and the GV oocytes were collected using a glass needle with a mouth pipette. MII oocytes were collected from the oviducts of female mice 13 h after injection with CARD HyperOva and 7.5 IU human chorionic gonadotropin (hCG; ASKA Pharmaceutical, Tokyo, Japan) 48 h apart. The oviductal wall was punctured using a 26G needle to collect cumulus-oocyte complexes in 20 µL potassium simplex optimization medium (KSOM; Kyudo) drops covered with liquid paraffin.

DNA vector construction and mRNA synthesis

Complementary DNA for mouse *Lamp1* (accession number NM_001317353) or *Atp6v1a* (accession number NM_001358204) was amplified using PCR with High-fidelity Taq Polymerase, KOD FX Neo (Toyobo, Osaka, Japan), and a mouse ovary cDNA library as a template (Genostaff, Tokyo, Japan). The amplicon was then subcloned into the entry vector pDONR221 and transferred into the destination vectors pDEST-CMV-C-EGFP[22] (a gift from Robin Ketteler (Addgene plasmid # 122844; *http://n2t.net/addgene:122844*; RRID: Addgene_122844); for *Lamp1*) or pDest-mCherry-N1[23]. (a gift from Robin Shaw (Addgene plasmid # 31907; *http://n2t.net/addgene:31907*; RRID: Addgene_31907); for *Atp6v1a*) using Gateway recombination cloning technology. The following primer combinations were used for cloning: 5'-GCGCACAAGTTTGTACAAAAAAGCAGGCTGCCACCATGGCGGCCCCCGGCG-3' and 5'-GCGCACCACTTTGTACAAGAAAGCTGGGTTGATGGTCTGATAGCCGGCGTGACT -3' (for *Lamp1*), or 5'-GCGCACAAGTTTGTACAAAAAAGCAGGCTGCCACCATGGATTTCTCCAAGCTAC CC-3' and 5'-GCGCACCACTTTGTACAAGAAAGCTGGGTTGTCTTCAAGGCTACGGAATG-3' (for *Atp6v1a*). The cDNA

encoding *Lamp1-EGFP* or *Atp6v1a-mCherry* were amplified using the following primer combinations: 5'-CGCAAATGGGCGGTAGGCGTG-3' and 5'-TCCAGCAGGACCATGTGATCGC-3' (for *Lamp1-EGFP*), or 5'-CGCAAATGGGCGGTAGGCGTG-3' and 5'-TTGGTCACCTTCAGCTTGG-3' (for *Atp6v1a-mCherry*). RNA synthesis using each PCR amplicon as a template, poly-A tail addition, and mRNA purification were performed using an mMESSAGE mMACHINE T7 Ultra kit (Thermo Fisher Scientific) and MEGAclear transcription clean-up kit (Thermo Fisher Scientific), according to the manufacturer's protocols. Synthesized mRNAs were dissolved in RNase-free demineralized water at a concentration of 400 ng/μL and frozen in aliquots until use.

In vitro maturation, fertilization, and embryonic culture

IVM for the GV oocytes was conducted by washing the oocytes twice and culturing in alpha-modified Eagle's minimum essential medium (Thermo Fisher Scientific) containing 5% (vol/vol) fetal bovine serum (FBS), 0.1 IU/mL follicle-stimulating hormone (MSD, Tokyo, Japan), 1.2 IU/mL of hCG (ASKA Pharmaceutical), and 4 ng/mL of epidermal growth factor (Thermo Fisher Scientific) for 17 h at 37 °C under a 5% CO_2 atmosphere[24]. For *in vitro* fertilization, spermatozoa from a B6D2F1 epididymis were pre-incubated in a 100-μL modified human tubal fluid medium (Kyudo) drop covered with liquid paraffin and inseminated at a sperm concentration of 1.5×10^5 per mL for 1.5 h. Excess spermatozoa were washed out, and the oocytes were incubated in a 20-μL KSOM drop (Kyudo) for further development. IVM assays using latrunculin A and cytochalasin B were performed by transferring oocytes to medium drops containing each inhibitor or DMSO 4 h after the start of IVM (waiting for the completion of GVBD), as previously reported[16]. IVM media containing DMSO, latrunculin A, or cytochalasin B was prepared by diluting the stock solution (1:400), and the final concentration of the inhibitors was 10 μM. The embryonic culture assay using bafilomycin A_1 was conducted by transferring the PN-zygote into a 20-μL drop of KSOM containing 25 nM bafilomycin A_1 covered with liquid paraffin at 6 h post-fertilization (hpf). Embryos were transferred at 24, 48, and 72 hpf to freshly prepared KSOM containing bafilomycin A_1.

Immunostaining

Immunostaining of oocytes or embryos was performed as previously described[10]. Oocytes or embryos were cultured to the indicated stages and fixed in 4% paraformaldehyde (PFA; Nacalai Tesque) in phosphate-buffered saline (PBS) containing 0.1 mg/mL polyvinyl alcohol (PVA; Sigma-Aldrich; PVA/PBS) for 15 min at 25–27 °C. After fixation, the cells were permeabilized with PVA/PBS containing 0.1% Triton X-100 (Sigma-Aldrich) for 30 min at 25–27 °C and washed three times with PVA/PBS. After blocking with 10% FBS (Thermo Fisher Scientific) in PBS for 1 h at room temperature, the cells were incubated with the aforementioned primary antibodies (1:100 for all) overnight at 4 °C. Next, the cells were washed three times in PVA/PBS and incubated with anti-mouse, rat, or rabbit IgG secondary antibodies coupled with Alexa Fluor 488, 555, or 564 (1:200 for all; Thermo Fisher Scientific) at 25–27 °C for 2–4 h. Thereafter, the cells were incubated with PVA/PBS containing 10 μg/mL Hoechst 33342 (Dojindo) for 10 min and washed with fresh PVA/PBS a few times. Subsequently, control and nonspecific staining were performed by processing oocytes and embryos in the absence of primary antibodies. The oocytes and embryos were imaged in PVA/PBS microdrops in 35-mm glass-bottomed dishes (MatTek Corporation, Ashland, MA, USA). For each position, confocal images at 81 *z*-axis planes with 1-μm increments were acquired on an IX-71 inverted microscope (Olympus Corporation, Tokyo, Japan) equipped with a CSU W-1 confocal scanner unit (Yokogawa Electric Corporation) using a 60× silicone immersion lens UPLSAPO60XS (Olympus Corporation).

LysoTracker/LysoSensor staining of oocytes and generation of ratio images

Acidic organelles in the oocytes were visualized using LysoTracker Red DND-99 and LysoSensor Green DND-189 (Thermo Fisher Scientific) according to the manufacturer's instructions. Briefly, the oocytes or embryos at target stages for one experimental round were obtained simultaneously and incubated in a large drop of reaction mixture (KSOM containing 1/10,000 Magic Red stock solution dissolved in DMSO and 1/1,000 LysoSensor Green DND-189 stock solution dissolved in DMSO) for 30 min at 37 °C under 5% CO_2 in a humidified atmosphere in liquid paraffin in a 35-mm glass-bottom dish (MatTek Corporation). Subsequently, confocal images at 41 *z*-axis planes with 2-μm increments were obtained using a CSU W-1 spinning disk confocal microscope with a 30× silicone immersion lens UPLSAPO30XS (Olympus Corporation). Acquisition conditions for fluorescence excited by 470-nm (LysoSensor) and 555-nm (LysoTracker) lasers were determined in preliminary experiments to be almost 1:1 intensities between the two wavelengths for cytosolic punctate structures in the 2-cell embryo. Further generation of ratio images for LysoTracker/LysoSensor fluorescence were carried out using Fiji software[25]. Averaged intensity projection was carried out, determining background intensity of each field by subtracting the averaged intensities of four cellular blank regions from the whole image. Then, 32-bit ratio images for LysoTracker/LysoSensor fluorescence of cytosolic regions were generated by processing images with "Math/Divide" function in Fiji, and "fire" look up table images were converted to RGB images.

Magic Red/LysoSensor staining

Intracellular cathepsin activity was assayed in oocytes or embryos using Magic Red Cathepsin B or Cathepsin L detection kits (ImmunoChemistry Technologies LLC, Davies, CA, USA) according to the manufacturer's instructions. Briefly, the oocytes or embryos at target stages for one experimental round were obtained simultaneously and incubated in a large drop of reaction mixture (KSOM containing 1/250 Magic Red stock solution dissolved in DMSO and 1/1,000 LysoSensor Green DND-189 stock solution dissolved in DMSO) for 25 min at 37 °C under 5% CO_2 in a humidified atmosphere in liquid paraffin in a 35-mm glass-bottom dish (MatTek Corporation). Thereafter, Hoechst 33342 (10 μg/mL) was added to the drop to a final concentration of 10 μg/mL, and incubated for 5 min. Subsequently, oocytes or embryos at the same stage were collected, and confocal images at 41 *z*-axis planes with 2-μm increments for both 470-nm (LysoSensor) and 555-nm (Magic Red) lasers were obtained on a CSU W-1 spinning disk confocal microscopy using a 30× silicone immersion lens UPLSAPO30XS (Olympus Corporation).

In-resin CLEM and electron microscopy

In-resin CLEM was performed as previously described with some modifications[14, 15]. Briefly, oocytes were fixed in 4% PFA and 0.025% glutaraldehyde (GA). After permeabilization with 50 μg/mL digitonin (Nacalai Tesque) and 0.02% Triton X-100, oocytes were washed with PVA/PBS three times and incubated with PBS containing 10% (w/v) FBS (Thermo Fisher Scientific) for 1 h at room temperature. Thereafter, oocytes were incubated with PVA/PBS containing primary antibody overnight at 4 °C. After incubation with a secondary antibody in PVA/PBS for 2 h, oocytes were fixed in 4% PFA and 2.5% GA, embedded in 1.5% agarose, stained with osmium tetroxide, dehydrated with graded ethanol solutions (QY1), and embedded in epoxy resin (Oken Shoji, Tokyo, Japan). Ultrathin sections of Epon-embedded oocytes (100-nm thickness) were prepared using a Leica UC6 ultramicrotome (Leica, Nussloch, Germany) and placed on glass coverslips. Subsequently, fluorescence microscopy images of the sections were obtained using a Nikon A1RHD25 confocal laser scanning microscope with a NIS-Elements software (Nikon, Tokyo, Japan). Electron microscopic images were observed using a Helios Nanolab 660 FIB-SEM instrument (FEI Company, Hillsboro, USA).

For conventional electron microscopy, the oocytes were fixed in the presence of 2% PFA and 2.5% GA and stained with osmium tetroxide. After dehydration with ethanol, the oocytes were embedded in epoxy resin, as described above. Sections were cut at a thickness of 100 nm using a UC6 ultramicrotome, mounted on glass coverslips, stained with uranyl acetate and lead citrate, and observed under a Regulus8240 scanning electron microscope (Hitachi High-Tech Corporation, Tokyo, Japan).

Serial semi-thin sections and 3D reconstruction of toluidine blue-positive structures

Serial semi-thin sections were cut at a thickness of 300 nm using a UC6 ultramicrotome and mounted on glass slides. Next, the sections were stained with 1% toluidine blue/0.1 M PB, and images were obtained using a BX50 light microscope (Olympus Corporation). Serial toluidine blue-stained images were aligned using FIJI (National Institutes of Health, MD, USA) with plugin-linear stack alignment using SIFT (LSAS), and 3D reconstruction was performed using Amira software (Thermo Fisher Scientific).

Microinjection into the oocytes

Microinjection of mRNA into GV oocytes was performed as previously described[26,27]. Briefly, antral follicles were harvested in FHM medium containing 250 μM of dbcAMP using 26G needles (Terumo). After dissociating the cumulus cells by pipetting, the oocytes were transferred to medium supplemented with 250 μM of dbcAMP and 10 μM of cytochalasin B (Sigma-Aldrich). Thereafter, mRNA injection into the oocytes was performed using a piezo-micromanipulator (Primetech, Tokyo, Japan) with a glass capillary needle. The mRNA concentrations were 50 and 100 ng/μL for *V1A-mCherry* and *Lamp1-EGFP*, respectively. The oocytes were washed three times and used for IVM. Microinjection of mRNA into zygote stage embryo (at 3–4 hpf) was carried out as previously described[10]. The concentration of mRNA was the same as that in the GV oocytes.

Time-lapse confocal imaging of oocytes/embryos

Low-invasive confocal fluorescence imaging of oocytes/embryos was performed as previously described[28,29,30] with slight modifications. Briefly, on an inverted microscope IX-71 (Olympus Corporation) equipped with a CSU W-1 confocal scanner unit (Yokogawa Electric Corporation), an incubation chamber (Tokai Hit, Fujinomiya, Japan) was set at 37 °C on the microscope stage, with a gas mixture of 5% CO_2 introduced into the chamber at 150 mL/min. Oocytes/embryos were placed in 8 μL of IVM medium or KSOM drops covered with liquid paraffin (Nacalai Tesque) in 35-mm glass-bottomed dishes (MatTek Corporation). Subsequently, confocal images at 41 *z*-axis planes with 2-μm increments for excitation lasers of 470- and 555-nm from an LDI-7 Laser Diode Illuminator (89North, Williston, VT, USA) were obtained every 30 or 60 min during IVM or embryonic culture observation, respectively, through optimized band-pass filters using 30× silicone immersion lens UPLSAPO30XS (Olympus Corporation).

Three-dimensional object analysis

Series of confocal images with 81 z-axis planes with 1-μm increments for LAMP1 immunostaining were used for 3D object analysis. Fields to analyze were cropped for each oocyte/embryo, and the upper and lower end of LAMP1 fluorescent signals in the cytosol were examined to determine the center plane (middle height) of the cell. The cellular region in the center plane was used for masking and determination of the geometric center (as a 3D center) of each oocyte. Deletion of the signals from the polar body or zona pellucida was carried out manually. Objects were profiled using the 3D object counter plugin[31] of Fiji software[25], to measure the number, volume, geometric center of each object, and mean distance from the geometrical center of the object to its surface. Thresholding was carried out after background subtraction using the Fiji software, manually applying intensities of 600–1200 as threshold to recognize objects separately. Signals on

PM were eliminated both via size filtering (0–5000 μm^3) of the 3D object counter plugin and manual erasing. The distal distance of each object from the 3D center of the oocyte was used for distribution analysis to avoid underestimation of the distance of large ELYSA. This was calculated by adding the distance from the 3D center of the oocyte to the geometric center of each object and the mean distance from the geometrical center of the object to its surface. Distance calculation and generation of bar graphs were carried out using Excel 2016 software (Microsoft, Redmond, WA, USA). Object-based colocalization analysis for the punctate structures were performed using the JACoP plugin in the ImageJ Fiji software[31]. Confocal z-stack images of multiple wave length for LAMP1 and LC3 or RAB5 antibodies were acquired for each oocyte as above, and object-based colocalization was examined by identifying coincidence of geometric centers of LC3 or RAB5 objects overlapping on LAMP1 objects. All of the LAMP1-positive 3D objects were listed with the 3D object counter plugin applied with same threshold, and the colocalized LAMP1-positive objects were identified and analyzed using the Excel 2016 software.

Analysis of microscopic images and movies

Analysis of the acquired images, including the generation of a line plot of intensity, adjustment of intensity, and generation of montage images at a uniform intensity, was performed using Fiji software[25]. To enhance the images, a Gaussian Blur filter (at a sigma radius of 1) and auto-adjustment of the intensity were applied to the stack of images. To adjust the intensity, auto-adjustment of the intensity was applied to each image. The movies were concatenated using Premiere Pro software (Adobe, San Jose, CA, USA).

Statistics and reproducibility

Sample sizes were estimated based on previous studies using similar experiments, and results from preliminary experiments were examined to ensure statistical power more than 0.8 using statistical power analysis in the G*Power software[32]. Statistical analyses and generation of dot plot graphs were performed using GraphPad Prism 8 (GraphPad Software, Boston, MA, USA). The significance of difference among groups were compared using one-way ANOVA and Tukey's multiple comparison test. The experimenters were not blinded because of a limitation in the availability of experienced personnel.

Data availability

The data supporting the findings of this study are available from the corresponding authors upon request.

Acknowledgements

We would like to thank Editage (*www.editage.jp*) for English language editing.

Additional information

Materials availability statement

The materials supporting the findings of this manuscript are available from the corresponding authors upon reasonable request.

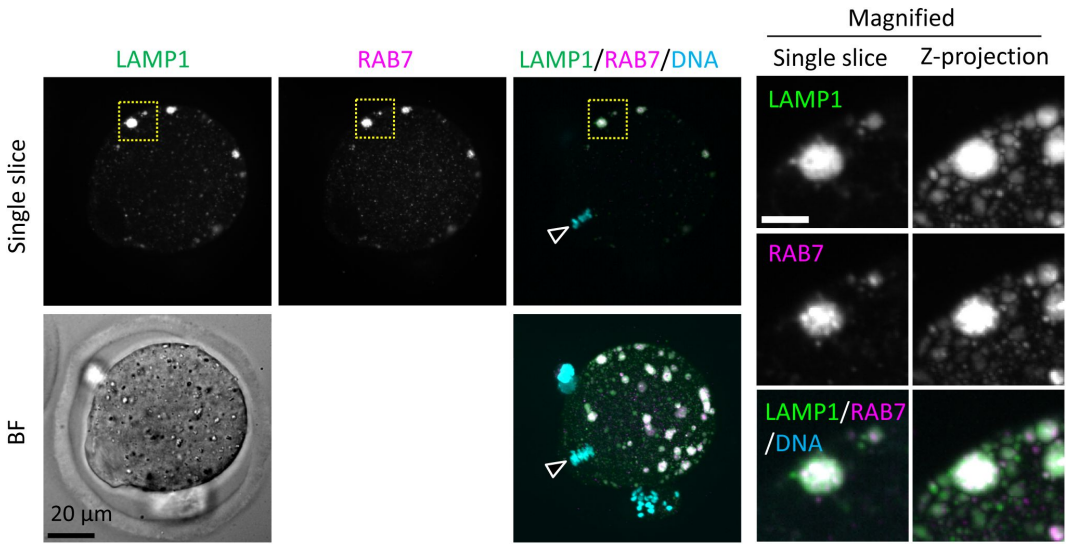

Supplementary Fig. 1.

Endosomes and lysosomes form giant structures in the periphery of the oocyte plasma membrane

MII oocytes were fixed and co-stained with anti-RAB7 and anti-LAMP1 antibodies. The schematic diagram indicates the location of oocyte chromosomes and the metaphase plate in the MII oocytes. Maximum intensity projection of confocal images at an axial scan range of 80 µm is shown as Z-projection images. Arrowheads indicate the positions of oocyte chromosomes.

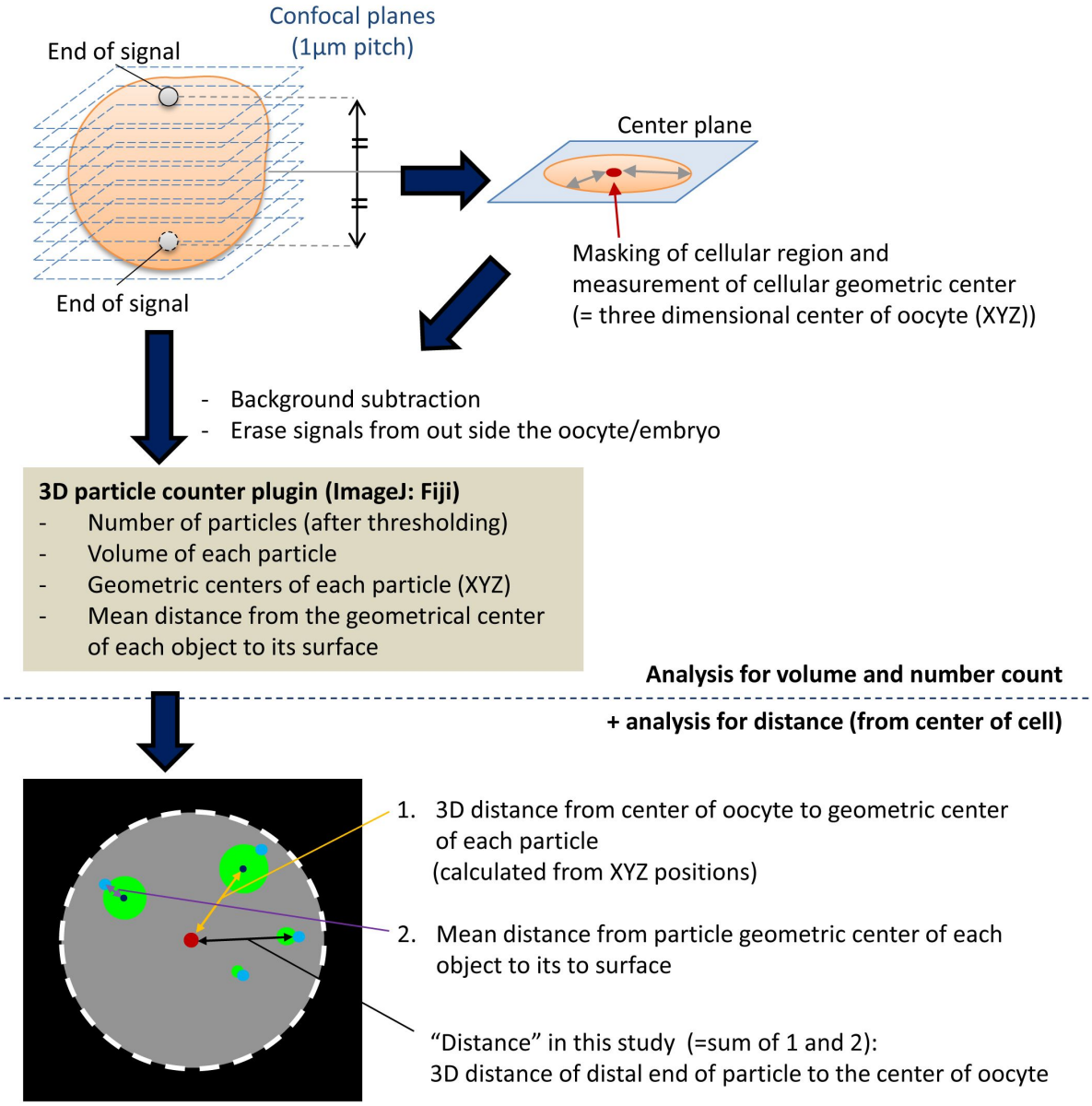

Supplementary Fig. 2.

Schemes of the three-dimensional particle analysis in this study

Oocytes/embryos were fixed and stained, and three-dimensional images were acquired as serial z-stack images using confocal microscopy. Fields to analyze were cropped for each oocyte/embryo, and the upper and lower end of LAMP1 fluorescent signals in cytosol were examined and used to determine the center plane of the cell. The cellular region in the center plane was used for masking and determination of the geometric center (as a 3D center of the oocyte). Deletion of the signals from the polar body or zona pellucida was carried out manually. Signals on PM were eliminated by both size exclusion of 3D particle counter plugin in Fiji software and by manual erasing. The distal distance of each particle from the 3D center of the oocyte was used for the distribution study to avoid underestimation of the distance of large ELYSA particle, which was calculated by adding the 3D distance from the center of cell to the geometric center of the particle and the mean diameter of the particle.

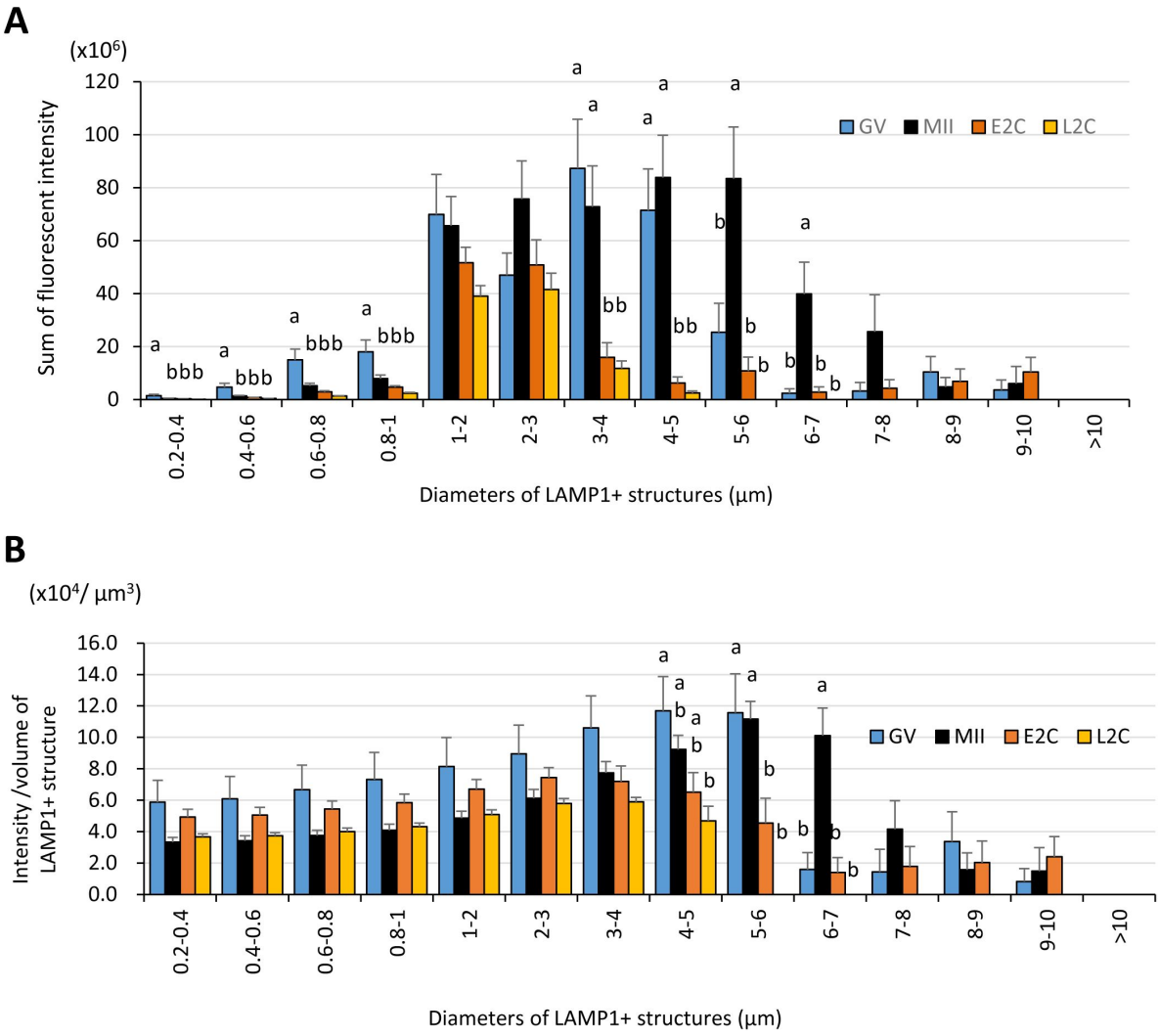

Supplementary Fig. 3.

Large LAMP1-positive structures exhibit high fluorescent intensity, especially in MII oocytes

Germinal vesicle (GV) oocytes, MII oocytes, early 2-cell (E2C: 24 hpf), and late 2-cell (L2C: 40 hpf) embryos were fixed and stained with anti-LAMP1 antibody. Reconstituted three-dimensional objects for the LAMP1-positive objects in 9 to 10 oocytes for each stage from more than three independent experiments were further analyzed for size and fluorescent intensity. The sorting by size (indicated by the diameters of spheres calculated from volumes) was carried out by thresholding the fluorescent intensity prior to measuring intensity. (A) Total fluorescent intensity of LAMP1-positive objects with different sizes. (B) Intensity/volume ratios of LAMP1-positive objects with different sizes. Groups with different letters are significantly different ($P < 0.05$, one-way ANOVA and Tukey's multiple comparison test). Error bars indicate SEM.

Supplementary Fig. 4.

Giant structures in MII oocytes were immunostained with anti-RAB7 and LAMP1 antibodies after glutaraldehyde (GA) fixation

MII oocytes were fixed with 0.025% GA and co-stained with anti-RAB5/RAB7 and anti-LAMP1 antibodies. Single-section images from confocal observation are shown.

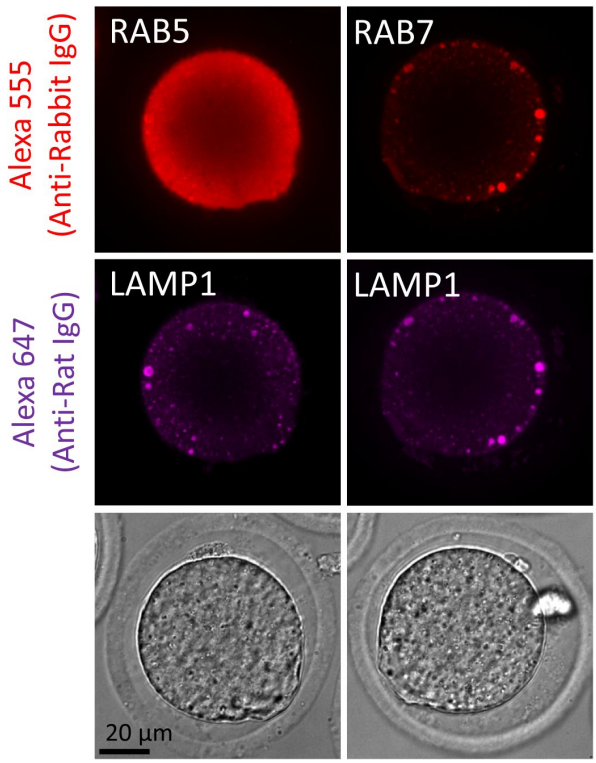

Supplementary Fig. 5.

Toluidine blue-positive structures in MII oocytes show similar localization patterns to the ELYSA

Aligned serial toluidine blue-stained light microscopic images were stacked and three-dimensionally reconstructed by inversing the intensity and adjusting it to be transparent.

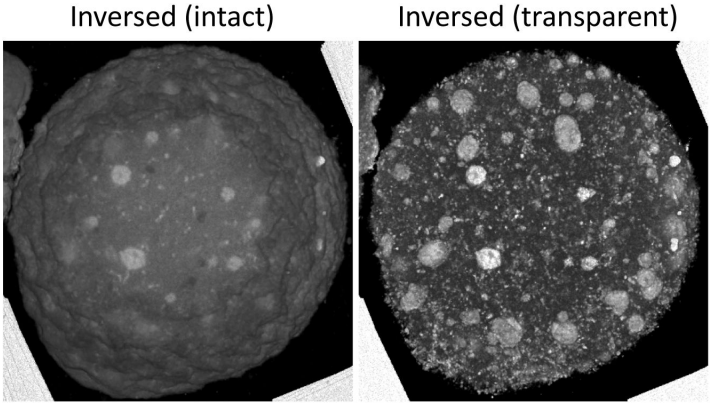

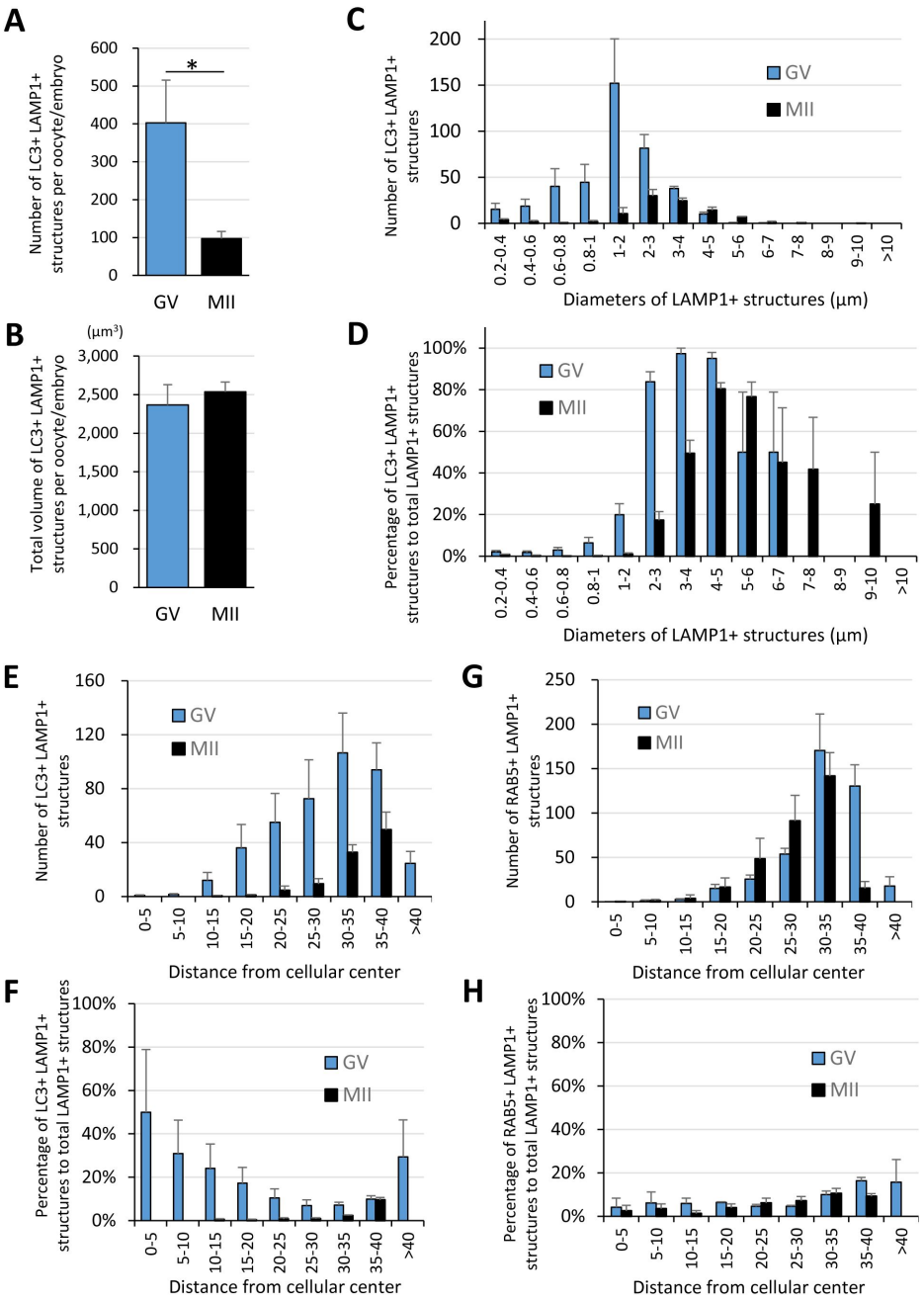

Supplementary Fig. 6.

LC3 signals colocalize with LAMP1 signals in a size-dependent manner

GV and MII oocytes stained with anti-LAMP1 antibody and anti-LC3 or anti-RAB5 antibody were reconstituted three-dimensionally for their objects positive for the target proteins, and 3 to 4 oocytes for each stage were further analyzed for number, size, and distribution. (A, B) Averaged total numbers or total volumes of the double-positive objects for LC3 and LAMP1 per oocyte/embryo, respectively. (C, D) Average numbers or percentage of total LAMP1-positive objects of the double-positive objects for LC3 and LAMP1 after sorting of the objects by size (indicated by the diameters of spheres calculated from volumes), respectively. (E, F) The double-positive objects for LC3 and LAMP1 were sorted by distance from the three-dimensional geometrical center of the oocyte. Average numbers or percentages of total LAMP1-positive objects are indicated, respectively. (G, H) The double-positive objects for RAB5 and LAMP1 were sorted by distance from the three-dimensional geometrical center of the oocyte. Average numbers or percentages of total LAMP1-positive objects are indicated, respectively. Significance was examined using a two-tailed Student's t-test, assuming equal variances between groups; the significance is indicated with asterisks ($P < 0.05$). Error bars indicate SEM.

Supplementary Fig. 7.

An early endosome marker RAB5 is localized within the ELYSA in the presence of inhibitors for cytoskeletons

GV oocytes were incubated for *in vitro* maturation (IVM) for 18 h with or without inhibitors of polymerized actin (10 μM latrunculin A or cytochalasin B) or tubulin (20 μM nocodazole), and fixed and co-stained with anti-RAB5 and anti-LAMP1 antibodies. Maximum intensity projection of confocal images at an axial scan range of 80 μm is shown as Z-projection images. Magnified regions are indicated by yellow boxes. DNA was stained with Hoechst 33342. Arrowhead and asterisk indicate the metaphase plate and first polar body, respectively.

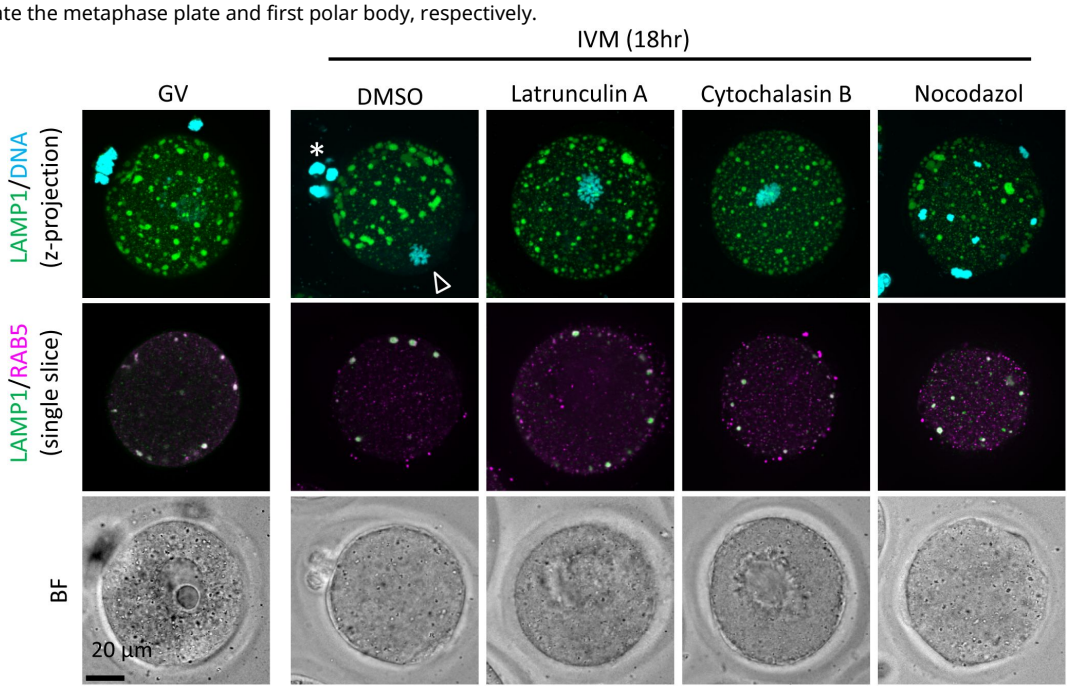

Supplementary Fig. 8.

Treatment with inhibitors for cytoskeltons affected the number of LAMP1-positive objects but not their volume

GV oocytes were incubated for *in vitro* maturation (IVM) for 18 h with or without actin polymerization inhibitors (10 μM latrunculin A or cytochalasin B) or a tubulin inhibitor (20 μM nocodazole), then fixed and co-stained with anti-LC3 and anti-LAMP1 antibodies. The reconstituted objects for LAMP1-positive objects in 10 oocytes for each treatment from more than three independent experiments were analyzed for the number, size, and distribution. (A) Average total object number per oocyte. (B) Total volumes of the objects. Groups with different letters are significantly different ($P < 0.05$, one-way ANOVA and Tukey's multiple comparison test). Error bars indicate SEM.

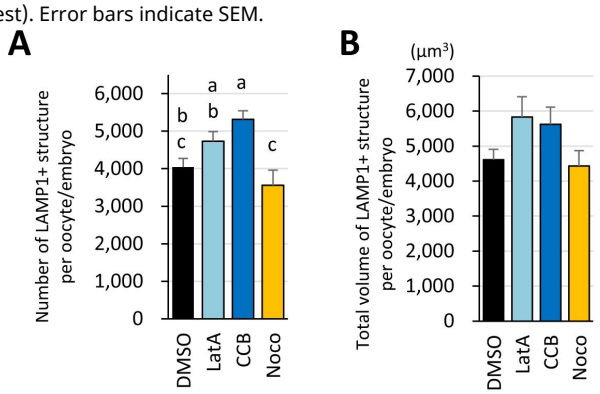

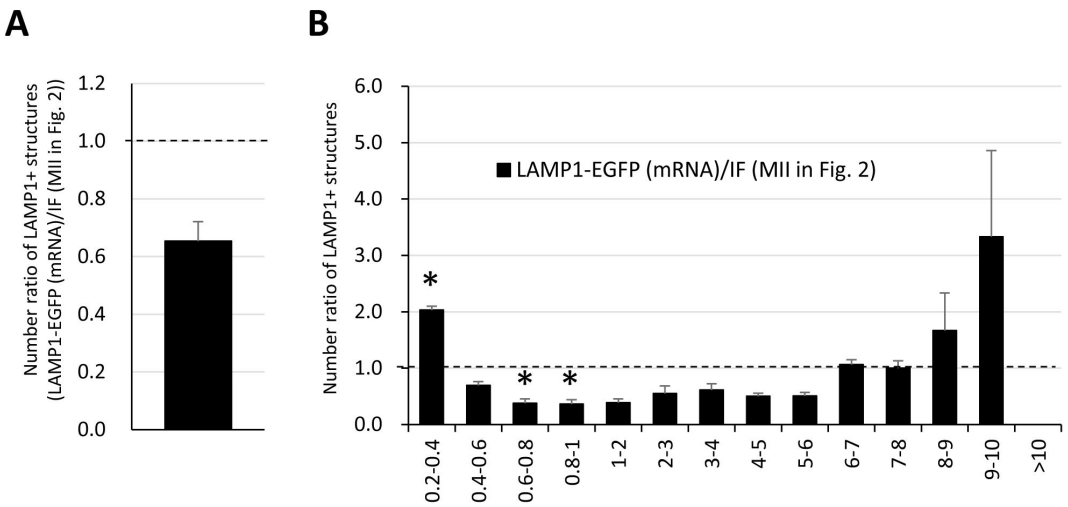

Supplementary Fig. 9.

Number and distribution of large LAMP1-EGFP structures do not significantly differ from intrinsic LAMP1 examined with immunofluorescence

After the *in vitro* maturation (IVM) for 18 h, LAMP1-EGFP fluorescence injected as mRNA in the GV stage was compared with intrinsic LAMP1 detected with an anti-LAMP1 antibody. The reconstituted objects for LAMP1-positive structures from 3 oocytes were compared with those from immunofluorescent analysis in **Figure 2** for the number and size. (A) Ratio of average numbers of total LAMP1-positive to that of MII in **Figure 2**. (B) Ratios of numbers of total LAMP1-positive structures sorted by size (indicated by the diameters of spheres calculated from volumes). Significance was examined using a two-tailed Student's t-test, assuming equal variances between groups; the significance is indicated with asterisks ($P < 0.05$). Error bars indicate SEM.

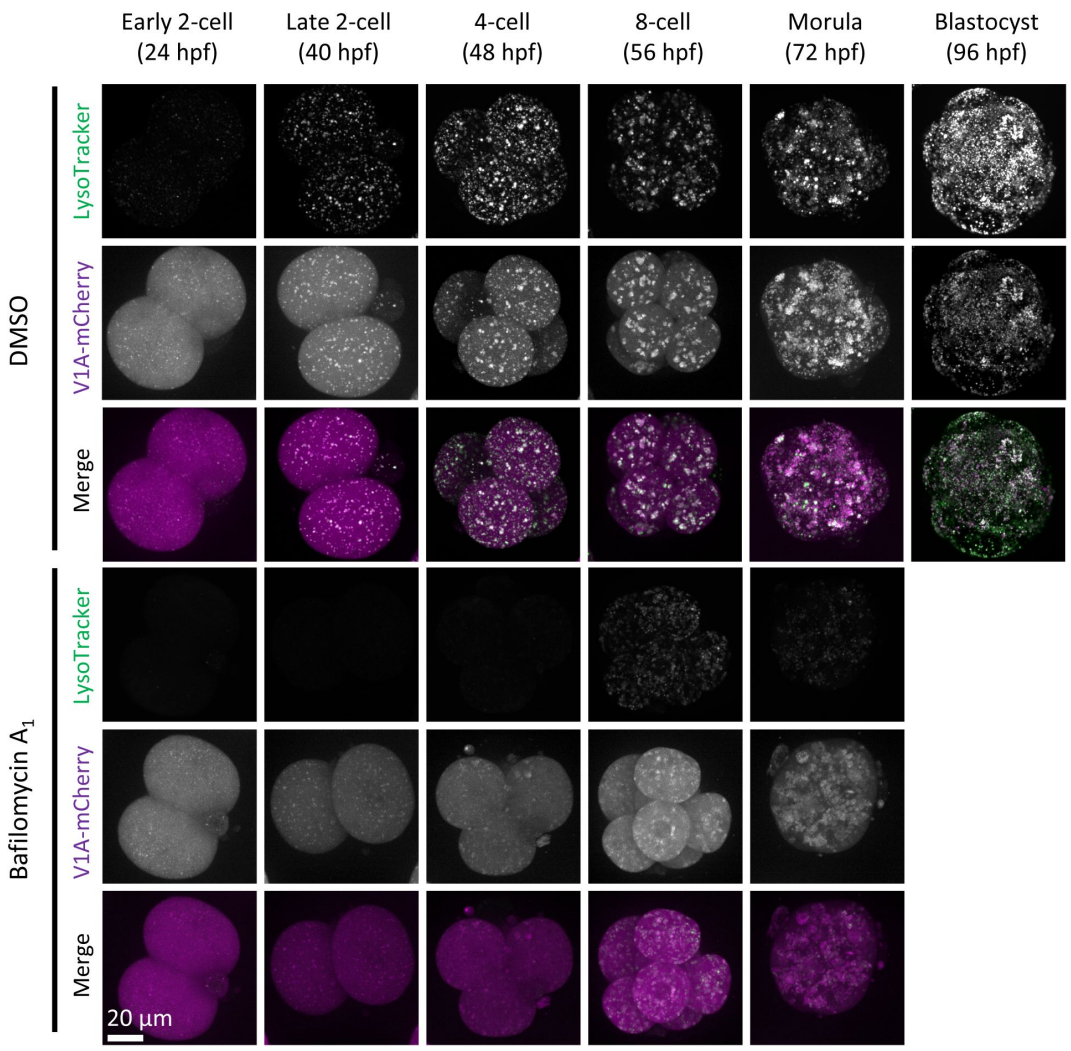

Supplementary Fig. 10.

LysoTracker-positive punctate structures colocalized with V1A-mCherry

Embryos were injected with V1A-mCherry mRNA (at 3 hpf) and cultured with or without bafilomycin A_1 and stained with LysoTracker Green at the indicated time points. Maximum intensity projection of confocal images at an axial scan range of 80 µm is shown as Z-projection images.

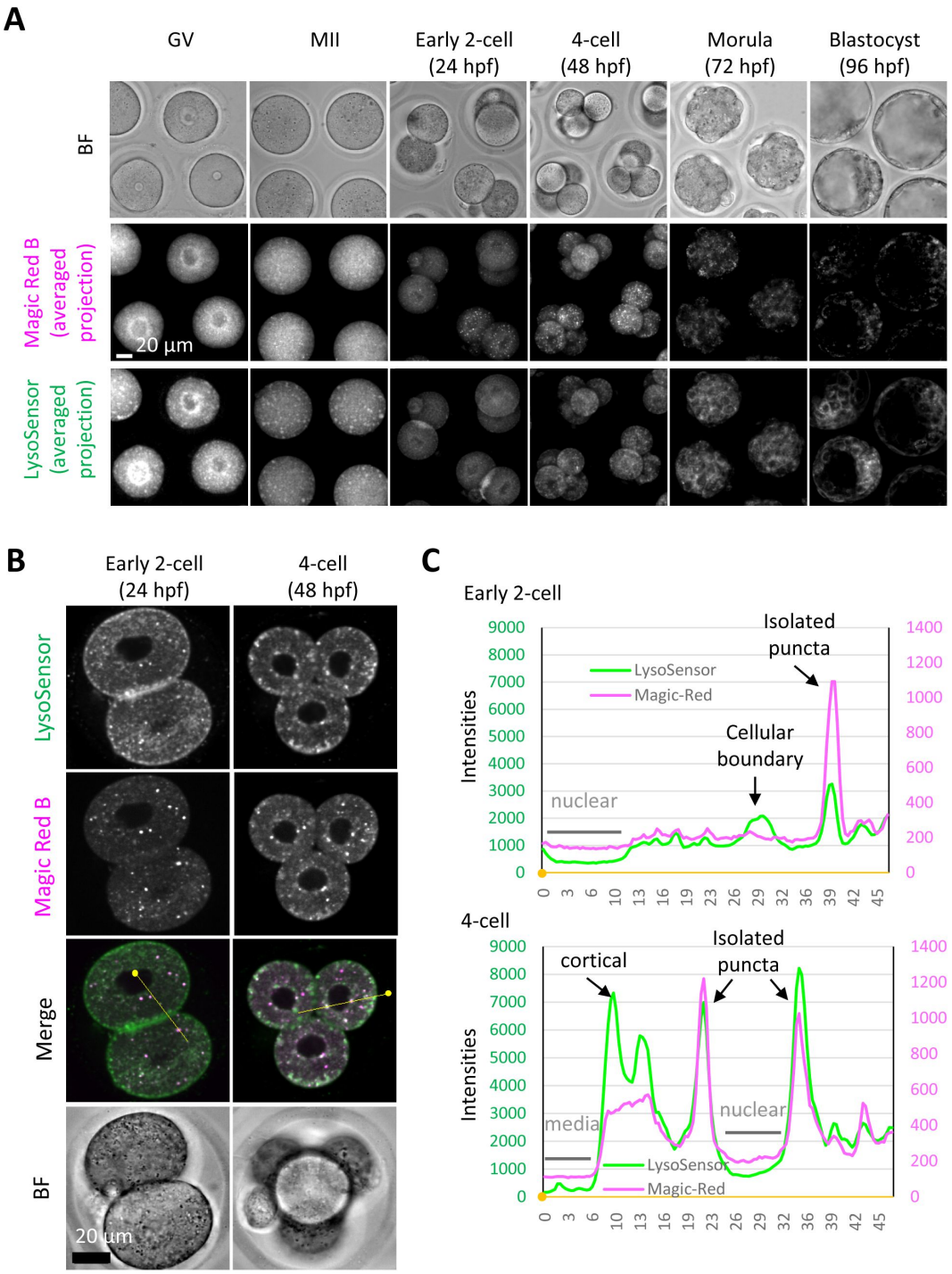

Supplementary Fig. 11.

Magic Red Cathepsin B staining in GV and MII oocytes showed higher cytoplasmic signals but similar intensity in isolated punctate structures to developing embryos

Oocytes and embryos at the indicated stages were collected and stained with Magic Red Cathepsin B solution in the same drop of medium. (A) Averaged intensity projection of confocal images at an axial scan range of 80 µm is shown as Z-projection images. (B) Early 2-cell and 4-cell embryos were stained in the same drop for LysoSensor Green and Magic Red Cathepsin B staining analysis, and confocal images were acquired. (C) Fluorescent intensities of LysoSensor and Magic Red on the yellow lines indicated in (B) are indicated by a line plot. Small, filled dots indicate the origin (0 µm) in distance.

Funding

This study was supported by the Japan Society for the Promotion of Science KAKENHI (Grant Numbers 19H05711, 20H00466, 24H02031 to K. Sato, 21H02435, 22H02872, and 22H04652 to I. Tanida, and 20K22744 to J. Yamaguchi), Takeda Science Foundation to K. Sato (Grant Number 2024095741), the Mochida Memorial Foundation for Medical and Pharmaceutical Research, Takeda Science Foundation (Grant Number 2022093867), and The Cell Science Research Foundation to Y. Satouh. This work was partly supported by the Project for Elucidating and Controlling Mechanisms of Aging and Longevity from the Japan Agency for Medical Research and Development (AMED 21gm5010003 to Y. Uchiyama., 22gm1710001 s0201 and 23gm1710001s0202 to I. Tanida) and by the MEXT-supported Program for the Strategic Research Foundation at Private Universities (to Y. Uchiyama), and the Center of Genomic and Regeneration Medicine, Juntendo University Graduate School of Medicine (to Y. Uchiyama and I. Tanida).This work was partly supported by the joint research program of the Institute for Molecular and Cellular Regulation, Gunma University (24014 to I. Tanida and K. Sato).

Author contributions

Y.S. and K.S. established the essential research concepts for this study. Y.S. and T.T. performed immunostaining and assays using mouse oocytes/embryos. I. T., J. Y., and Y. U. performed the CLEM experiments and analyses. Y. S. and K. S. prepared the manuscript.

Additional files

Video 1. *MII oocytes were fixed and co-stained with anti-RAB5 and anti-LAMP1 antibodies. A series of the confocal images with a height of 80 μm is shown from top to bottom.*

Video 2. *A series of continuous toluidine blue-stained light microscopic images of the same oocyte (top half) reconstructed to 3D. Chromosomes in the images obtained were segmented blue, toluidine blue-positive structures were segmented yellow, and oocyte PM was segmented white.*

Video 3. *GV oocytes were injected with the mixture mRNA solution for Lamp1-EGFP and V1A-mCherry, and incubated for IVM. Time-lapse movie of EGFP fluorescence of a representative oocyte is indicated as maximum intensity projection of confocal images with a height of 80 μm. Magnified perinuclear regions in Fig. 5 are indicated by a box. The timestamp indicates the time after IVM started.*

Video 4. *GV oocytes were injected with V1A-mCherry mRNA and incubated for 18 h for IVM in the presence of LysoSensor green. Fluorescent images of a representative oocyte which matured to MII stage is presented. A series of the confocal images of 81 slices with a height of 80 μm is shown from top to bottom.*

Video 5. *Embryos were injected with V1A-mCherry mRNA at 3 hpf and incubated for further embryogenesis in the presence of LysoSensor Green during embryonic development. A time-lapse movie of a representative embryo is shown (maximum intensity projection of confocal images at a height of 80 μm).*

References

1. Li L, Zheng P, Dean J 2010) **Maternal control of early mouse development** *Development* **137**:859–870

2. Verlhac MH, Terret ME, Pintard L 2010) **Control of the oocyte-to-embryo transition by the ubiquitin-proteolytic system in mouse and C. elegans** *Curr Opin Cell Biol* **22**:758–763

3. Jiang ZY, Fan HY 2022) **Five questions toward mRNA degradation in oocytes and preimplantation embryos: when, who, to whom, how, and why?** *Biol Reprod* **107**:62–75

4. Schier AF 2007) **The maternal-zygotic transition: death and birth of RNAs** *Science* **316**:406–407

5. Shin SW, et al. 2013) **Mouse zygote-specific proteasome assembly chaperone important for maternal-to-zygotic transition** *Biol Open* **2**:170–182

6. Shin SW, et al. 2010) **Inhibition of the ubiquitin-proteasome system leads to delay of the onset of ZGA gene expression** *J Reprod Dev* **56**:655–663

7. Sato K 2022) **Multiple roles of endocytosis and autophagy in intracellular remodeling during oocyte-to-embryo transition** *Proc Jpn Acad Ser B Phys Biol Sci* **98**:207–221

8. Birgisdottir AB, Johansen T. 2020) **Autophagy and endocytosis - interconnections and interdependencies** *J Cell Sci* **133**

9. Tsukamoto S, Kuma A, Murakami M, Kishi C, Yamamoto A, Mizushima N 2008) **Autophagy is essential for preimplantation development of mouse embryos** *Science* **321**:117–120

10. Morita A, Satouh Y, Kosako H, Kobayashi H, Iwase A, Sato K 2021) **Clathrin-mediated endocytosis is essential for the selective degradation of maternal membrane proteins and preimplantation development** *Development* **148**

11. Satouh Y, Sato K 2023) **Reorganization, specialization, and degradation of oocyte maternal components for early development** *Reprod Med Biol* **22**

12. Bohnert KA, Kenyon C 2017) **A lysosomal switch triggers proteostasis renewal in the immortal C. elegans germ lineage** *Nature* **551**:629–633

13. Tsukamoto S, et al. 2013) **Functional analysis of lysosomes during mouse preimplantation embryo development** *J Reprod Dev* **59**:33–39

14. Tanida I, Yamaguchi J, Suzuki C, Kakuta S, Uchiyama Y 2023) **Application of immuno- and affinity labeling with fluorescent dyes to in-resin CLEM of Epon-embedded cells** *Heliyon* **9**

15. Mitsui S, Yamaguchi J, Suzuki C, Uchiyama Y, Tanida I 2023) **TUNEL-positive structures in activated microglia and SQSTM1/p62-positive structures in activated astrocytes in the neurodegenerative brain of a CLN10 mouse model** *Glia* **71**:2753–2769

16. FitzHarris G, Marangos P, Carroll J 2007) **Changes in endoplasmic reticulum structure during mouse oocyte maturation are controlled by the cytoskeleton and cytoplasmic dynein** *Dev Biol* **305**:133–144

17. Schulz KN, Harrison MM 2019) **Mechanisms regulating zygotic genome activation** *Nat Rev Genet* **20**:221–234

18. Satouh Y, et al. 2023) **Endosomal-lysosomal organellar assembly (ELYSA) structures coordinate lysosomal degradation systems through mammalian oocyte-to-embryo transition** *bioRxiv* https://doi.org/10.1101/2023.12.29.573616

19. Zaffagnini G, et al. 2024) **Mouse oocytes sequester aggregated proteins in degradative super-organelles** *Cell* **187**:1109–1126

20. Tsukamoto S, et al. 2014) **Fluorescence-based visualization of autophagic activity predicts mouse embryo viability** *Sci Rep* **4**

21. Takeo T, Nakagata N 2015) **Superovulation using the combined administration of inhibin antiserum and equine chorionic gonadotropin increases the number of ovulated oocytes in C57BL/6 female mice** *PLoS One* **10**

22. Agrotis A, Pengo N, Burden JJ, Ketteler R 2019) **Redundancy of human ATG4 protease isoforms in autophagy and LC3/GABARAP processing revealed in cells** *Autophagy* **15**:976–997

23. Hong TT, et al. 2010) **BIN1 localizes the L-type calcium channel to cardiac T-tubules** *PLoS Biol* **8**

24. Morohaku K, et al. 2016) **Complete in vitro generation of fertile oocytes from mouse primordial germ cells** *Proc Natl Acad Sci U S A* **113**:9021–9026

25. Schindelin J, et al. 2012) **Fiji: an open-source platform for biological-image analysis** *Nat Methods* **9**:676–682

26. Umeda R, et al. 2020) **Structural insights into tetraspanin CD9 function** *Nat Commun* **11**

27. Kato K, et al. 2016) **Structural and functional insights into IZUMO1 recognition by JUNO in mammalian fertilization** *Nat Commun* **7**

28. Nozawa K, Satouh Y, Fujimoto T, Oji A, Ikawa M 2018) **Sperm-borne phospholipase C zeta-1 ensures monospermic fertilization in mice** *Sci Rep* **8**

29. Satouh Y, Nozawa K, Yamagata K, Fujimoto T, Ikawa M 2017) **Viable offspring after imaging of Ca2+ oscillations and visualization of the cortical reaction in mouse eggs** *Biol Reprod* **96**:563–575

30. Satouh Y, Inoue N, Ikawa M, Okabe M 2012) **Visualization of the moment of mouse sperm-egg fusion and dynamic localization of IZUMO1** *J Cell Sci* **125**:4985–4990

31. Bolte S, Cordelieres FP 2006) **A guided tour into subcellular colocalization analysis in light microscopy** *J Microsc* **224**:213–232

32. Faul F, Erdfelder E, Lang AG, Buchner A 2007) **G*Power 3: a flexible statistical power analysis program for the social, behavioral, and biomedical sciences** *Behav Res Methods* **39**:175–191

Author information

Yuhkoh Satouh
Laboratory of Molecular Traffic, Institute for Molecular and Cellular Regulation, Gunma University, Maebashi, Japan
ORCID iD: 0000-0001-9207-9374

For correspondence: yuhkohs@gunma-u.ac.jp

Takaki Tatebe
Laboratory of Molecular Traffic, Institute for Molecular and Cellular Regulation, Gunma University, Maebashi, Japan
ORCID iD: 0009-0003-8998-3567

Isei Tanida
Department of Cellular and Molecular Neuropathology, Juntendo University Graduate School of Medicine, Tokyo, Japan
ORCID iD: 0000-0001-8999-3990

Junji Yamaguchi
Department of Cellular and Molecular Neuropathology, Juntendo University Graduate School of Medicine, Tokyo, Japan
ORCID iD: 0009-0002-9199-9931

Yasuo Uchiyama
Department of Cellular and Molecular Neuropathology, Juntendo University Graduate School of Medicine, Tokyo, Japan

Ken Sato
Laboratory of Molecular Traffic, Institute for Molecular and Cellular Regulation, Gunma University, Maebashi, Japan
ORCID iD: 0000-0002-1034-5091

For correspondence: sato-ken@gunma-u.ac.jp

Editors

Reviewing Editor
Noboru Mizushima
University of Tokyo, Tokyo, Japan

Senior Editor
Wei Yan
Washington State University, Pullman, United States of America

Reviewer #1 (Public review):

Satouh et al. report giant organelle complexes in oocytes and early embryos. Although these structures have often been observed in oocytes and early embryos, their exact nature has not been characterized. The authors named these structures "endosomal-lysosomal organelles

form assembly structures (ELYSAs)". ELYSAs contain organelles such as endosomes, lysosomes, and probably autophagic structures. ELYSAs are initially formed in the perinuclear region and then seem to migrate to the periphery in an actin-dependent manner. When ELYSAs are disassembled after the 2-cell stage, the V-ATPase V1 subunit is recruited to make lysosomes more acidic and active. The ELYSAs are most likely the same as the "endolysosomal vesicular assemblies (ELVAs)", reported by Elvan Böke's group earlier this year (Zaffagnini et al. doi.org/10.1016/j.cell.2024.01.031). However, it is clear that Satouh et al. identified and characterized these structures independently. These two studies could be complementary. Although the nature of the present study is generally descriptive, this paper provides valuable information about these giant structures. Since the ELYSA described in this paper and ELVA proposed by Elvan Böke appear to be the same structure, it would be helpful to the field if the two groups discuss unifying the nomenclature in the future.

Comments on latest version:

In this revised manuscript, the authors have provided additional data supporting their conclusions and also revised the text to more accurately reflect the experimental results.

https://doi.org/10.7554/eLife.99358.2.sa2

Reviewer #2 (Public review):

Satouh et al report the presence of spherical structures composed of endosomes, lysosomes and autophagosomes within immature mouse oocytes. These endolysosomal compartments have been named as Endosomal-LYSosomal organellar Assembly (ELYSA). ELYSAs increase in size as the oocytes undergo maturation. ELYSAs are distributed throughout the oocyte cytoplasm of GV stage immature oocytes but these structures become mostly cortical in the mature oocytes. Interestingly, they tend to avoid the region which contain metaphase II spindle and chromosomes. They show that the endolysosomal compartments in oocytes are less acidic and therefore non-degradative but their pH decreases and become degradative as the ELYSAs begin to disassemble in the embryos post fertilization. This manuscript shows that lysosomal switching does not happen during oocyte development, and the formation of ELYSAs prevent lysosomes from being activated. Structures similar to these ELYSAs have been previously described in mouse oocytes (Zaffagnini et al, 2024) and these vesicular assemblies are important for sequestering protein aggregates in the oocytes but facilitate proteolysis after fertilization. The current manuscript, however, provides further details of endolysosomal disassembly post fertilization. Specifically, the V1-subunit of V-ATPase targeting to the ELYSAs increases the acidity of lysosomal compartments in the embryos. This is a well-conducted study and their model is supported by experimental evidence and data analyses.

Comments on revisions:

This revised version of the manuscript has addressed most of my concerns.

https://doi.org/10.7554/eLife.99358.2.sa1

Author response:

The following is the authors' response to the original reviews.

> ***Public Reviews:***

Reviewer #1 (Public Review):

In this manuscript, Satouh et al. report giant organelle complexes in oocytes and early embryos. Although these structures have often been observed in oocytes and early embryos, their exact nature has not been characterized. The authors named these structures "endosomal-lysosomal organelles form assembly structures (ELYSAs)". ELYSAs contain organelles such as endosomes, lysosomes, and probably autophagic structures. ELYSAs are initially formed in the perinuclear region and then migrate to the periphery in an actin-dependent manner. When ELYSAs are disassembled after the 2-cell stage, the V-ATPase V1 subunit is recruited to make lysosomes more acidic and active. The ELYSAs are most likely the same as the "endolysosomal vesicular assemblies (ELVAs)", reported by Elvan Böke's group earlier this year (Zaffagnini et al. doi.org/10.1016/j.cell.2024.01.031). However, it is clear that Satouh et al. identified and characterized these structures independently. These two studies could be complementary. Although the nature of the present study is generally descriptive, this paper provides valuable information about these giant structures. The data are mostly convincing, and only some minor modifications are needed for clarification and further explanation to fully understand the results.

Reviewer #2 (Public Review):

Satouh et al report the presence of spherical structures composed of endosomes, lysosomes, and autophagosomes within immature mouse oocytes. These endolysosomal compartments have been named as Endosomal-LYSosomal organellar Assembly (ELYSA). ELYSAs increase in size as the oocytes undergo maturation. ELYSAs are distributed throughout the oocyte cytoplasm of GV stage immature oocytes but these structures become mostly cortical in the mature oocytes. Interestingly, they tend to avoid the region which contains metaphase II spindle and chromosomes. They show that the endolysosomal compartments in oocytes are less acidic and therefore non-degradative but their pH decreases and becomes degradative as the ELYSAs begin to disassemble in the embryos post-fertilization. This manuscript shows that lysosomal switching does not happen during oocyte development, and the formation of ELYSAs prevents lysosomes from being activated. Structures similar to these ELYSAs have been previously described in mouse oocytes (Zaffagnini et al, 2024) and these vesicular assemblies are important for sequestering protein aggregates in the oocytes but facilitate proteolysis after fertilization. The current manuscript, however, provides further details of endolysosomal disassembly post-fertilization. Specifically, the V1-subunit of V-ATPase targeting the ELYSAs increases the acidity of lysosomal compartments in the embryos. This is a well-conducted study and their model is supported by experimental evidence and data analyses.

Reviewer #3 (Public Review):

Fertilization converts a cell defined as an egg to a cell defined as an embryo. An essential component of this switch in cell fate is the degradation (autophagy) of cellular elements that serve a function in the development of the egg but could impede the development of the embryo. Here, the authors have focused on the behavior during the egg-to-embryo transition of endosomes and lysosomes, which are cytoplasmic structures that mediate autophagy. By carefully mapping and tracking the intracellular location of well-established marker proteins, the authors show that in oocytes endosomes and lysosomes aggregate into giant structures that they term Endosomal LYSosomal organellar Assembl[ies] (ELYSA). Both the size distribution of the ELYSAs and their position within the cell change during oocyte meiotic maturation and after fertilization. Notably, during maturation, there is a net actin-dependent movement towards the periphery of the oocyte. By the late 2-cell stage, the ELYSAs are beginning to disintegrate. At this stage, the

> *endo-lysosomes become acidified, likely reflecting the activation of their function to degrade cellular components.*
>
> *This is a carefully performed and quantified study. The fluorescent images obtained using well-known markers, using both antibodies and tagged proteins, support the interpretations, and the quantification method is sophisticated and clearly explained. Notably, this type of quantification of confocal z-stack images is rarely performed and so represents a real strength of the study. It provides sound support for the conclusions regarding changes in the size and position of the ELYSAs. Another strength is the use of multiple markers, including those that indicate the activity state of the endo-lysosomes. Altogether, the manuscript provides convincing evidence for the existence of ELYSAs and also for regulated changes in their location and properties during oocyte maturation and the first few embryonic cell cycles following fertilization.*
>
> *At present, precisely how the changes in the location and properties of the ELYSAs affect the function of the endo-lysosomal system is not known. While the authors' proposal that they are stored in an inactive state is plausible, it remains speculative. Nonetheless, this study lays the foundation for future work to address this question.*
>
> *Minor point: l. 299. If I am not mistaken, there is a typo. It should read that the inhibitors of actin polymerization prevent redistribution from the cytoplasm to the cortex during maturation.*
>
> *Minor point: A few statements in the Introduction would benefit from clarification. These are noted in the comments to the authors.*

We sincerely appreciate the editorial board of *eLife* and the reviewers for their helpful and constructive comments on our manuscript. We are pleased that the reviewers acknowledged that we identified and characterized this assembly structure independently. In the revised manuscript, we have carefully considered the reviewers' comments and conducted additional analysis to address each of them.

Regarding the typographical errors, we revised the description to fit with our findings and the reviewers' comments. We also found that the primer sequence was correct, and we carefully checked the accuracy of the entire manuscript.

We hope that the revised version will now be deemed suitable for publication in *eLife*.

> ***Recommendations for the authors:***
>
> ***Reviewer #1 (Recommendations For The Authors):***
>
> *Q. 1) The authors state in the Abstract that ELYSAs contain autophagosome-like membranes in the outer layer. However, this seems to be just speculation based on the LC3 staining results and is not directly shown. Are there autophagosome-like double membrane structures in ELYSAs?*

We appreciate this comment. We also agree with this concern; however, it was difficult to assert that they are autophagosomes based on the observation of the electron micrographs. For this reason, we rephrased it to be "Most ELYSAs are also positive for an autophagy regulator, LC3." (lines 33). In addition, we revised the notation to LC3-positive structures in the Result and Discussion section (line 165-169, 286).

> *Q. 2) The data in Figure 2A, showing a decrease in the number of LAMP1 structures, seems to contradict the data in Figure 1B, showing an apparent increase in LAMP1 structures. Please explain this discrepancy. If the authors did not count structures just below the plasma membrane, please explain the rationale for this.*

We really appreciate the valuable comment. Regarding the number of LAMP1-positive structures, it is not suitable for comparison with Figure 1B, etc., as pointed out by the reviewer, since the distribution of the LAMP1 signal differs from plane to plane. To avoid any potential confusion, we added new images of the Z-projection of the immunostained images that can better reflect the number of positive structures in the whole oocyte/embryo in Figure 2.

In addition, as the reviewer pointed out, there is a technical difficulty in measuring the LAMP1-positive signal on the plasma membrane or just below it. We explained how and why we had to delete plasma membrane signals in our response #21.

> *Q. 3) The actin dependence is not observed in Figure 5C. What is the difference between Figure 5C and 5E? Please explain further.*

We apologize for the lack of clarity; Figures 5C and 5E show the average number of LAMP1-positive structures (5C) and the percentage of the sum of granule volumes in LAMP1 positive structure (5E), respectively, after classifying the LAMP1 positive granules by their diameters.

We removed Figure 5E for the sake of conciseness since we already mentioned a similar fact in Figure 5C. To clarify the corresponding explanations, we moved figures that were not classified by diameter to Supplementary Figure 8 to improve readability. Moreover, we have rewritten the main text on lines 200–211.

> *Q. 4) While the actin inhibitors reduce the number of peripheral LAMP1 structures (Figure 5F), they do not affect their number in the central region (Figure 5G). How can the authors conclude that actin inhibitors inhibit the migration of LAMP1 structures?*

We appreciate the comment. As pointed out, the number of large LAMP1-positive structures in the medial region did not change. Therefore, we have avoided the description that ELYSAs migrate from the middle region to the cell periphery and have unified the description of whether large structures in the periphery occur. Please refer to the subsection title (line 188), the following descriptions (lines 189–199), the related description in the Results (lines 200–211), and the title and the legend of Figure 5.

> *Q. 5) The authors show that the V1A subunit associates with the surface of LAMP1 structures as punctate structures (Figure 6B). What are these V1A-positive structures? Is V1A recruited to some specific domains of ELYSAs, or are V1A-positive active lysosomes recruited to ELYSAs? Please provide an interpretation of these data. The phrase "The V1-subunit of V-ATPase is targeted to these structures" (line 262) is not appropriate because it is indistinguishable whether only the V1 subunits are recruited or active lysosomes containing the V1 subunit are recruited.*

Thank you for the valuable comment. Indeed, our analysis, including the analysis of Fig. 8 described on line 262, did not clarify whether free V1A-mCherry molecules accessed the ELYSA periphery or whether lysosomes with V1A-mCherry molecules newly merged into the ELYSA. Therefore, we added this interpretation to lines 232–234 of the Results and revised the Discussion as "The number of membrane structures positive for V1A-mCherry increase upon ELYSA disassembly, indicating further acidification of the endosomal/lysosomal compartment" (lines 292–294).

> *Q. 6) Why did the authors use LysoSensor as a marker for ELYSA instead of LAMP1 in Figure 8 and 9? Some reasons should be given.*

There is a clear technical reason for this: when LAMP1-EGFP was expressed in a zygote, it was largely migrated to the plasma membrane before and after the 2-cell stage, making it difficult to capture the change of ELYSAs. To circumvent this difficulty, we used Lysosensor to visualize ELYSAs instead of LAMP1-EGFP. This explanation was added to lines 258–260.

> *Q. 7) In Figure 9A, it is not clear whether the activity of LysoSensor-positive structures is lower at this stage compared to other stages. It may be shown in Figure S7, but the data are not clearly visible. A direct comparison would be ideal.*

A new analysis similar to that shown in Fig. 9 for early 2-cells and 4-cells was performed and added to Figure S7. To support direct comparison, the ranges of axes were set to be similar.

As a result, the quantified MagicRed signal on the isolated LysoSensor-positive punctate structure in MII oocyte was nearly the same as that in early 2-cells and 4-cells. In early 2-cells, LysoSensor gave a signal at the cellular boundary, where MagicRed staining was not observed, confirming that MagicRed activity is higher in the interior than in the cell periphery in post-fertilization embryos. We have included an additional description in the main text (lines 280–282).

> *Q. 8) In the phrase "pregnant mare serum gonadotropin or an anti-inhibin antibody" (line 382), is "or" correct?*

When inducing superovulatory stimulation, an anti-inhibin antibody (distributed as CARD HyperOva) can be used as a substitute for PMSG (after additional stimulation with hCG), which results in the production of eggs of similar quality to those of PMSG. This was used in most experiments. To amend the lack of clarity, a reference (Takeo and Nakagata Plos One, 2015) was added to the description of HyperOva (line 417).

> *Q. 9) In almost all graphs, please indicate what the X-axis is indicating (not just "number") so that readers can understand what number is being represented without reading the legends.*

We revised the axis titles in all figures.

> *Q. 10) Since grayscale images provide better contrast than color images, it is recommended that single-color images be shown in grayscale.*

We replaced all single-color images with grayscale images.

> ***Reviewer #2 (Recommendations For The Authors):***
>
> *Specific comments:*
>
> *Q. 11) Figure 1 and S1- Both Rab5 and Rab7 co-localize with LAMP1. However, there seems to be a lot of LAMP1-free Rab5 dots as compared to the Lamp1-free Rab7. As a result, LAMP1 and Rab7 are co-localized more frequently than LAMP1 and Rab5 (video1). Could it be that early endosomes (Rab5+) are yet to be incorporated into ELYSAs? If so, a brief discussion of this phenomenon would be nice.*

Thank you very much for the comment. We agree with the reviewer's interpretation. In accordance with this suggestion, we clearly stated in the main text: "Although small punctate structures that are RAB5-positive but LAMP1-negative also spread over the cytosol, most giant structures were positive for RAB5 and LAMP1 (Video 1)" (lines 91–93). In the Discussion section, a brief statement was included: "Considering the large number of RAB5-positive and

LAMP1-negative punctate structures in MII oocytes, these layers may also reflect the assembly mechanism of the ELYSA" (lines 318–320).

> *Q. 12) Video 3 (and Figure 6) clearly shows the dynamics of LAMP1-labelled vesicles during maturation, which is impressive. In contrast to the live cell imaging after LAMP1 mRNA injection, Figure 1 used anti-LAMP1 Ab to detect endogenous levels of LAMP1. It appears that mRNA microinjection causes LAMP1 overexpression causing more (but smaller) vesicles to form. It should be easy to quantify and compare the vesicles in Figure 1 and 6*

We appreciate the comment. As mentioned, injections of EGFP-LAMP1 mRNA are useful for the visualization of LAMP1 dynamics during the maturation phase from GV to MII by live cell imaging, which is not feasible with immunostaining. However, the fluorescence emitted by EGFP-LAMP1 is only a few tenths of that of antibody staining, and because of the technical difficulty of microinjection into GV oocytes, the signal-to-noise ratio sufficient for imaging was merely one in ten oocytes. In addition, live cell imaging of oocytes in Figure 6 had to be carried out with very low excitation light exposure to reduce the toxicity. It was also performed with a low magnification lens and a longer step size in the z-axis. For these reasons, in examining the point raised, we performed an additional 3D object analysis, in the same way as in Figure 2, on the data of IVM oocytes injected with EGFP-LAMP1 mRNA using the same lens as in Figure 1 and with a longer exposure time than in live imaging. The results were compared with the MII data of Figures 1 and 2.

As a result, as shown in the new Figure S8, more objects with a diameter of 0.2–0.4 μm were found than in the immunostaining data, which fits the reviewer's point. In addition, the counts were lower for the 0.6–1.0 μm diameter, but there was no significant difference in the number of larger LAMP1 positive structures corresponding to the ELYSA size. We consider that this was appropriate for the original purpose of characterizing the ELYSA formation process. A description of these points has been added to lines 221–225.

> *Q. 13) In Figure 4A and B- Seems like not all LAMP1-positive structures were LC3-positive. Is there any size or location within the oocyte that determines LC3 positivity?*

We appreciate the valuable comment. To answer this comment, we proceeded with a new 3D object-based co-localization analysis on Lamp1 and LC3, determined the number, volume, and distribution within the oocyte, and incorporated the results as Supplementary Figure 6. To examine the positivity, we further analyzed the percentage of double-positive structures of all the LAMP1-positive structures. The results showed that their average diameter significantly shifted from 2.36 μm (GV) to 3.78 μm (MII). Moreover, it was clearly indicated that LAMP1-positive structures smaller than 2 μm in diameter are rarely positive for LC3. In terms of location, measuring the distance of the double positive structures from the oocyte center (the cellular geometric center) indicated that they tend to be observed at the periphery of both stages of oocytes (more than 80% in > 30 μm in the MII oocyte). Of note, no clear tendency of double positivity was observed. A description of these points has been added to lines 174–186.

> *Q. 14) In discussion, line 256- Small ELYSAs are formed in GV oocytes. Since you haven't checked the smaller-sized, growing oocytes, I suggest rephrasing this sentence as 'are present' rather than 'are formed'.*

We agree with the reviewer's suggestion and changed it to "present" (line 287).

> *Q. 15) Line 188- ELISA should instead be ELYSA*

Thank you for pointing this out. We have found a few more typographical errors, and all of them have been corrected (lines 213 and 321).

> ***Reviewer #3 (Recommendations For The Authors):***
>
> *Q. 16) Line 42: What do you mean by 'zygotic gene expression following the degradation of the cellular components of each maternal and paternal gamete'? ZGA requires this degradation? Please provide supporting references from the literature.*

We apologize for the confusing wording. We meant to say that both ZGA and degradation of parental components are required. To avoid misunderstanding, we have revised “zygotic gene expression as well as the degradation of the cellular components of each maternal and paternal gamete” and inserted a new reference (line 44).

> *Q. 17) 50: MII means metaphase II, not meiosis II.*

We corrected the clerical mistake (line 50).

> *Q. 18) 51: Define LC3.*

We added the definition of LC3 (line 51-52).

> *Q. 19) 60: 'lysosomal activity in oocytes is upregulated by sperm-derived factors as the oocytes grow and mature'. As written, the sentence implies that oocytes grow and mature after fertilization. This may be true for maturation, but I would be surprised to learn that there is growth of the oocyte after fertilization.*

We appreciate this valuable comment.

The *C. elegans* lives mainly as a hermaphrodite, which contains a couple of U-shaped gonad arms including the ovary, spermatheca and uterus in the body. Oocytes grow in the ovary and maturate upon receiving major sperm proteins secreted from sperms and ovulated to the spermatheca for fertilization. In 2017, Kenyon’s group reported that major sperm proteins act as sperm-secreted hormones to upregulates the lysosomal activity in oocytes during oocyte growth and maturation. We have revised our manuscript to avoid misunderstanding, to ' lysosomal activity in oocytes is upregulated by major sperm proteins secreted from sperms as the oocytes grow and mature '. (L. 61-66).

> *Q. 20) 94 and Figure 1B: While it is clear that many LAMP1 foci at the late 2-cell stage do not also contain RAB5, it seems that the majority of RAB5 loci also stain for LAMP1. This may be a minor point in the context of the paper but could be clarified.*

We could not easily agree with the suggestion because of the possibility that the images might give different impressions on each plane. Therefore, as a way to verify this point, we attempted to quantify the co-localization by reconstructing the 3D puncta information based on the two types of antibody staining data. Unfortunately, as shown in Fig. 1AB, Rab5 had a high cytoplasmic background, and although we were able to extract peaks, we could not reliably recalibrate the three-dimensional punctate structure (please refer to the new Supplementary Fig. 6). Therefore, co-localization on each other's punctate structure (LAMP1/RAB5 vs. RAB5/LAMP1) could not be verified. The validation using specific planes also showed large differences between planes, with overlapping punctate structures counted separately in adjacent planes, making reliable quantification difficult. This is an issue that will be addressed in the future.

On the other hand, the newly added Z-projection figure (Fig. 1AB) shows that RAB5-positive and LAMP1-negative punctate structures tend to accumulate along the LAMP1-positive punctate structures larger than 1 μm at the late 2-cell stage in all observed embryos; we added this statement on lines 99–101.

> *Q. 21) 100-102 and Figure 2A: Does the decrease in the total number of LAMP1 foci refer just to cytoplasmic or also to membrane foci? If the former, what was the reason for not including the membrane in the analysis?*

We appreciate the critical question. The LAMP1 signal on the plasma membrane interfered with the measurement of the signals just below the plasma membrane. The biological cause of this increased signal on the plasma membrane, as shown in Fig. 2E, seemed to be caused by the migration of the LAMP1 signals post-fertilization, which was also reported in a previous paper by Zaffagnini et al. (2024), published in *Cell*.

In our analysis, oocytes are giant cells, and confocal imaging has a technical limitation in obtaining the same fluorescent intensity along the z-axis. However, 3D-object analysis requires thresholding based on absolute values. As a result of this situation, the presence of the plasma membrane signal caused punctate structures located close to the membrane to be captured and recognized as a single, very large LAMP1-positive structure, resulting in the loss of the punctate structure that should be measured.

To avoid this issue, we have used several programs to correct the fluorescence difference along the z-axis; nonetheless, these attempts were unsuccessful. Therefore, as described in the Materials and Methods section, we applied only background subtraction at each z-position and then manually removed the plasma membrane signal (which was thin and continuous at the edges). Furthermore, when the plasma membrane and punctate structure signals overlapped, we paid attention not to remove the signals but to separate them. Thus, we believe that the decrease in the number and volume of LAMP1-positive structures after fertilization is still a phenomenon associated with the shift of LAMP1 to the plasma membrane.

> *Q. 22) Figure 2B, F, G: As the x-axis does not represent a continuous variable, adjacent data points should not be connected by a line. The histogram representations in A, C, and E are much easier to understand. I suggest presenting all data in this format.*

We revised the line graphs to bar graphs. Besides, to make the significance among populations clearer, the significances are now expressed using alphabetical indicators.

> *Q. 23) Figure 2B, C: It seems that the values for the different stages are expressed relative to the value at MII. Why not use the GV value at the base-line? This would follow the developmental trajectory of the oocyte/embryo more directly and would not (I believe) change the conclusions.*

We appreciated the comment. We meant to express that ELYSA develops most in the MII phase and that it decreases after fertilization, so considering the reviewer's suggestion, we expressed GV-MII changes based on GV and changes after fertilization based on the MII phase (Fig. 2C, D).

https://doi.org/10.7554/eLife.99358.2.sa0